8-2023

Investigating Mitochondrial Influence on the Rate of Anaerobic Glycolysis in an *in vitro* Model

Mackenzie Jenna' Taylor
Utah State University

Investigating Mitochondrial Influence On The Rate Of Anaerobic Glycolysis In An *in*

vitro Model

by

MACKENZIE JENNA' TAYLOR

A thesis submitted in partial fulfillment
of the requirements for the degree

of

MASTER OF SCIENCE

In

Food Sciences

Approved:

_____   _____
Sulaiman K. Matarneh, Ph.D.   Kara J. Thornton-Kurth, Ph.D.
Major Professor   Committee Member

_____   _____
Silvana Martini, Ph.D.   D. Richard Cutler, Ph.D.
Committee Member   Vice Provost of Graduate Studies

UTAH STATE UNIVERSITY
Logan, Utah

2023

ABSTRACT

Investigating Mitochondrial influence on the Rate of Anaerobic Glycolysis in an *in vitro*

Model

by

Mackenzie Taylor, Master of Science

Utah State University, 2023

Major Professor: Dr. Sulaiman Matarneh
Department: Nutrition, Dietetics, and Food Sciences

The rate of postmortem pH decline is a crucial factor in determining pork quality. A gradual decrease in postmortem muscle pH (~ pH 5.6 by 24 h) is associated with desirable pork quality characteristics. In contrast, rapid pH decline is the immediate cause of the pale, soft, and exudative (PSE) meat defect. The exact biochemical mechanisms controlling the rate of postmortem pH decline are unclear, but recent studies propose that mitochondria could influence the rate of postmortem pH decline by completing lactate dehydrogenase (LDH) for pyruvate. As such, we hypothesized that inhibiting pyruvate dehydrogenase (PDH) and pyruvate carboxylase (PC) may increase the rate of pH decline by providing more substrate for anaerobic glycolysis. We utilized an *in vitro* system simulating postmortem metabolism and incorporated CPI-613 and Avidin to inhibit PDH and PC, respectively. Four treatments were tested: 400 µM CPI-613, 1.5 U/ml Avidin, 400 µM CPI-613 + 1.5 U/ml Avidin, or diluent (control). Our findings indicated that CPI-613-containing treatments, with or without Avidin, resulted in decreased pH levels, increased lactate and glucose-6-phosphate accumulation, and enhanced glycogen degradation compared to the

control. In a follow-up experiment using a glucose tracer, we observed lower enrichment of tricarboxylic acid cycle intermediates in the CPI-613 treated samples. To test whether the acceleration of acidification in reactions containing CPI-613 was due to an increase in the activity of key regulatory enzymes of glycogenolysis and glycolysis, we evaluated the activities of glycogen phosphorylase, phosphofructokinase, and pyruvate kinase in the presence or absence of 400 µM CPI-613. The CPI-613 treatment did not elicit an alteration in the activity of these three enzymes. Overall, our findings support the hypothesis that inhibiting PDH can increase glycolytic flux and accelerate pH decline. The results of this study shed light on the biochemical mechanisms involved in postmortem muscle metabolism. However, further research is needed to fully elucidate the role of mitochondria in postmortem metabolism and its impact on meat quality.

(2 pages)

PUBLIC ABSTRACT

Investigating Mitochondrial Influence on the Rate of Anaerobic Glycolysis in an *in vitro*

Model

Mackenzie Taylor

The rate at which the muscle acidifies after an animal is harvested has a profound effect on the quality of the resulting pork. When acidification increases gradually, desirable pork quality characteristics are developed. In contrast, rapid acidification deteriorates pork quality, exemplified by the pale, soft, and exudative (PSE) pork defect. The rate of acidification is determined by the rate of anaerobic metabolism in postmortem muscle. Yet the processes controlling postmortem anaerobic metabolism are not well understood. Recent research suggests that mitochondria, the powerhouse of the cell, may influence this process by competing for substrate (pyruvate) with anaerobic metabolism, thereby reducing its rate. This study aimed to examine the role of mitochondria in post-harvest acidification of pork. We hypothesized that inhibiting mitochondrial ability to uptake pyruvate would increase the rate of acidification. To test this hypothesis, CPI-613 and Avidin, inhibitors of pyruvate dehydrogenase (PDH) and pyruvate carboxylase (PC), respectively, were used in lab settings mimicking postmortem muscle metabolism. Four treatments were tested: control, CPI-613, Avidin, and CPI-613 + Avidin. A similar follow-up study incorporated a tracer to track pyruvate's fate. The results showed that inhibition of PDH with CPI-613 increased anaerobic metabolism and decreased mitochondrial metabolite enrichment, evidenced by an increased rate of acidification and anaerobic metabolism compared to the control. No effect was observed in the PC-inhibited samples. These findings suggest that mitochondria could have a regulatory role on the rate of post-

harvest metabolism. Overall, the data support our hypothesis that inhibiting mitochondrial

ability to uptake pyruvate increases the rate of acidification.

DEDICATION

Dedicated to my parents, Brad and Lorie Taylor, for never giving up on me even if they didn't understand what I was doing.

ACKNOWLEDGMENTS

I would like to express my deepest gratitude to my mentor, Dr. Sulaiman Matarneh, for his guidance, support, and encouragement throughout my Master's program. His wisdom, expertise, and generosity have been instrumental in shaping me personally and my research skills. I would not be here today if it was not for him taking a chance on me. I would also like to sincerely thank my committee members, Dr. Kara Thornton-Kurth and Dr. Silvana Martini, for their constant advice and help throughout this process. Their advice for my research and professional background has helped me tremendously. Special thanks to Tara Black for her wonderful support throughout my program. I would like to mention a special mention to Dr. David Dang and Mr. Jared Buhler for helping train and support me at the beginning of my research journey. To my lab mate, Chandler Stafford, thank you for always having my back.

To my friends, Michelle, Diana, Luis, Carlos, Warren, Rafa, Melissa, and Nathan, I am so glad to have had you with me on this journey. I am forever thankful to you guys for the emotional support and constant love. Thank you for making me laugh when I really needed it.

Lastly, I want to express my deepest appreciation to my family, my parents, Brad and Lorie, and my siblings, Braden, Jorden, Najee, and Madison, for their unwavering love and support. Their constant encouragement and presence in my life have been the foundation of my personal and professional success. My family has always been my rock through the ups and downs, providing a sense of stability and comfort that has helped me navigate life's challenges. Their unconditional love has given me the confidence to pursue my dreams and

to never give up on myself. I would also like to mention my dog, Declan, as he helped me keep a smile on my face even during the hard times.

<div align="right">Mackenzie Taylor</div>

CONTENTS

LIST OF TABLES

LIST OF FIGURES

LIST OF ABBREVIATIONS

ADP = Adenosine diphosphate

AMP = Adenosine monophosphate

ATP = Adenosine triphosphate

ATPase = Adenosinetriphosphatase

DFD = Dark, firm, and dry

CS = Citrate synthase

ETC = Electron transport chain

FA = Formic acid

FAD = Flavin adenine dinucleotide

GAPDH = Glyceraldehyde 3-phosphate dehydrogenase

GC = Gas chromatography

GP = Glycogen phosphorylase

G6P = Glucose-6-phosphate

H^+ = Hydrogen ions

HAL = Halothane gene

IMP = Inosine monophosphate

LDH = Lactate dehydrogenase

LL = Longissimus lumborum

MFA = Metabolic flux analysis

MPC = Mitochondrial pyruvate carrier

MS = Mass spectroscopy

NADH = Nicotinamide adenine dinucleotide

PCA = Perchloric acid

PC = Pyruvate carboxylase

PDH = Pyruvate dehydrogenase

PK = Pyruvate kinase

PFK = Phosphofructosekinase

pH = Potential hydrogen

Pi = Inorganic phosphate

pI = Isoelectric point

PSE = Pale, soft, and exudative

RYR1 = Ryanodine receptor type 1

SR = Sarcoplasmic reticulum

TCA = tricarboxylic acid

T-tubule = Transvers-tubules

WHC = Water holding capacity

1. INTRODUCTION

After harvesting an animal, oxygen is no longer delivered to the muscle. Consequently, muscle energy metabolism shifts from aerobic to anaerobic in a futile attempt to maintain cellular ATP levels. During anaerobic metabolism, stored muscle glycogen is broken down to yield glucose-6-phosphate (G6P), which subsequently enters glycolysis to produce pyruvate, NADH, and ATP. Without oxygen, pyruvate is converted to lactate, while ATP is hydrolyzed by muscle ATPases to $ADP + P_i + H^+$ (Fig. 1). Due to the lack of circulation, lactate and H^+ accumulate in the muscle, leading to its acidification.
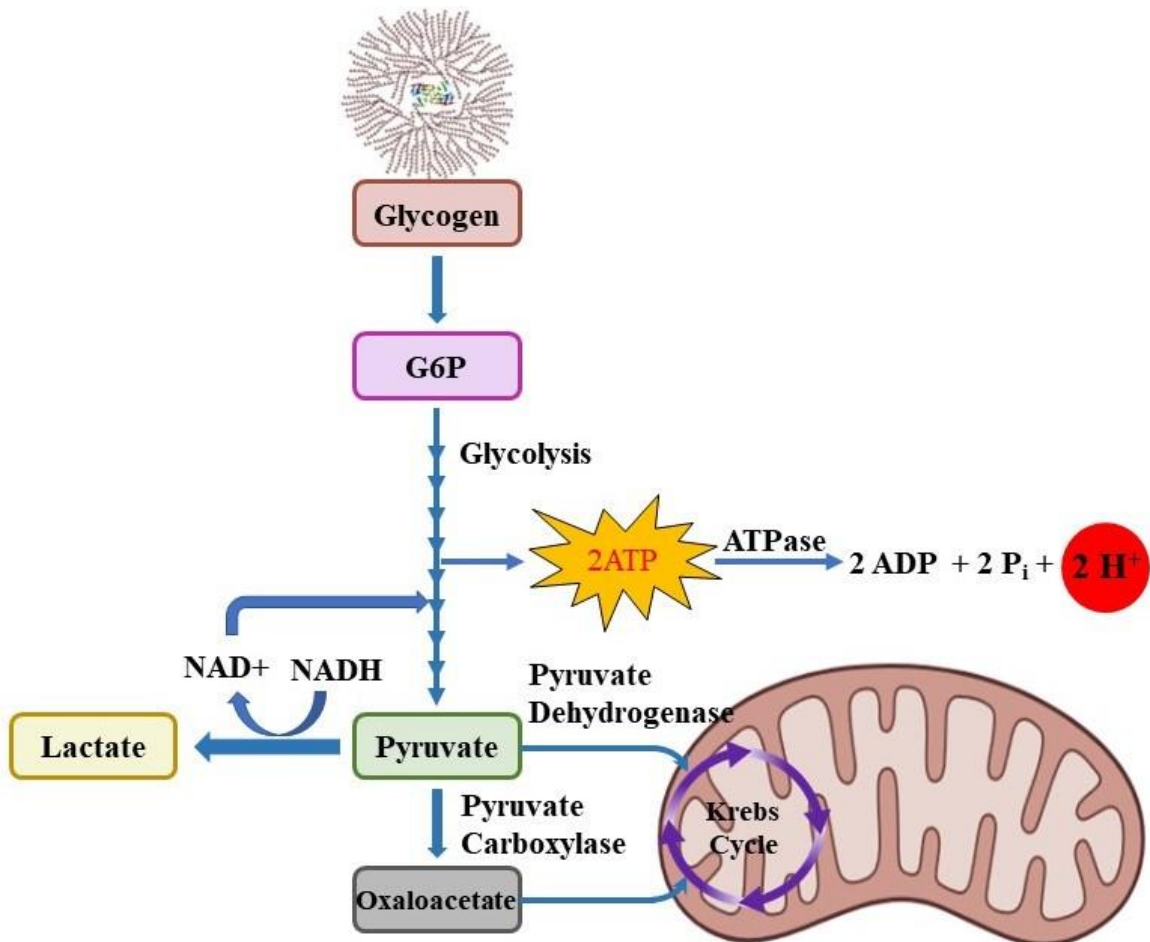
Fig. 1. A diagram showing the process of glycogen breakdown in an anaerobic environment.

Typically, pH of postmortem muscle drops gradually from ~ 7.2 to an ultimate pH around 5.6. The rate of postmortem pH decline, which reflects the intensity of postmortem metabolism, is one of the most significant factors affecting the development of meat quality attributes. Indeed, rapid pH decline is the direct reason for pale, soft, and exudative (PSE) meat, a defect observed predominantly in pork and poultry. In this case, muscle pH drops rapidly to a value around the ultimate pH of meat (~5.6) well before carcass chilling. The combination of low pH and high temperature exacerbates muscle protein denaturation and produces a product with a pale color, soft texture, and impaired water-holding capacity (WHC). Poor meat quality associated with PSE often results in its rejection by consumers, which causes an annual loss of several hundred million dollars for the US meat industry (Dong *et al.*, 1947).

The most traditional example of PSE is pork originating from pigs harboring Porcine Stress Syndrome (PSS), a genetic mutation in the ryanodine receptor type 1 (RYR1) gene that encodes the calcium release channel on the sarcoplasmic reticulum of muscle cells (Fujii *et al.*, 1991). The development of PSE meat in pigs carrying the RYR1 mutation has been attributed to an excessive release of calcium into the cytosol of muscle cells. Elevated intracellular calcium levels accelerate the rate of ATP hydrolysis and, subsequently, glycolysis and pH decline. Calcium also triggers a signaling cascade that promotes glycogen degradation, thereby providing more substrate for glycolysis (Matarneh, England, Scheffler, & Gerrard, 2017). Independent of genetics, exposure to acute stress prior to harvest contributes significantly to the prevalence of PSE by triggering similar physiological responses to that of the RYR1 mutant pigs (Matarneh, Silva, & Gerrard, 2021). Certainly, the incidence of PSE has been reduced through eradicating the RYR1

mutation and implementing proper animal handling practices and rapid carcass chilling techniques. Even so, PSE remains a major problem for the pork and poultry industries, with an incidence rate of up to 40% (Petracci, Bianchi, & Cavani, 2009). This suggests that other factors are involved in determining the rate of postmortem pH decline and PSE development.

Mitochondria are known for their essential role in ATP production through aerobic metabolism. Because the lack of oxygen hinders their respiration, the contribution of mitochondria to postmortem metabolism has been largely overlooked. However, recent studies suggest that mitochondria play a larger role than previously thought (Matarneh, Betine, Silva, Shi, & Gerrard, 2018; Matarneh, England, Scheffler, Yen, 2017; Matarneh, Yen, Bodmer, Kadi, & Gerrard, 2021). England *et al*. (2018) reported measurable oxygen concentrations in porcine muscle within the first 2 h postmortem, suggesting that oxidative phosphorylation could contribute to postmortem metabolism. In support of this construct, Matarneh *et al*. (2021) showed that mitochondria were capable of metabolizing a portion of pyruvate generated through glycolysis in an *in vitro* model simulating postmortem metabolism. The ability of mitochondria to metabolize pyruvate under postmortem conditions may reduce the pyruvate available for anaerobic glycolysis and, subsequently, the rate of pH decline. Indeed, the rate of pH decline is generally slower in muscles containing predominantly red fibers (rich in mitochondria) than those containing greater proportions of white fibers (poor in mitochondria). Thus, we hypothesized that mitochondria modulate the rate of postmortem glycolysis and pH decline by consuming a portion of glycolytic pyruvate. To investigate this hypothesis, we utilized an *in vitro* model mimicking postmortem metabolism and inhibited mitochondrial ability to utilize pyruvate

by blocking some of the pathways responsible for shuttling pyruvate into the mitochondria.

2. LITERATURE REVIEW

2.1. Skeletal Muscle Structure

Skeletal muscle is one of an animal's most dynamic and plastic tissues. It has a well-described architecture consisting primarily of muscle cells and three layers of connective tissue (Fig. 2). Epimysium is the connective tissue layer that surrounds the whole muscle. This layer protects the muscle and separates it from other tissues and organs. Muscles are made up of bundles (fascicles) of muscle cells that are encompassed by another connective tissue layer known as the perimysium. Finally, the endomysium, the innermost connective tissue layer, surrounds each individual muscle fiber. These connective tissue layers work together to provide support and transmit the force generated during muscle contractions to tendons or aponeurosis, allowing for movement.

Muscle fibers are thread-like, multinucleated cells ranging from several millimeters to several centimeters. Myofibrils are longitudinally oriented organelles found in muscle cells' sarcoplasm (cytoplasm of other cell types). These unique organelles are the contractile apparatuses of skeletal muscle. Transvers-tubules (T-tubules) are extensions of the sarcolemma (muscle cell membrane) that serve an essential role in transmitting nerve impulses into the interior of the cell (Schneider, 1994). The T-tubules interact with the sarcoplasmic reticulum (SR; the endoplasmic reticulum of muscle cells), an organelle responsible for the storage, release, and uptake of intracellular calcium (Al-Qusairi & Laporte, 2011; Endo, 1977). When an action potential travels down the T-tubules, it causes the release of calcium into the cytosol and, eventually, the initiation of muscle contraction. The energy requirements of skeletal muscle are mainly provided by the mitochondria, the

"powerhouse of the cell." In skeletal muscle, mitochondria are located underneath the sarcolemma (subsarcolemmal mitochondria) and between myofibrils (intermyofibrillar mitochondria) (Hoppeler, Vogt, Weibel, & Flück, 2003).

Myofibrils are made of an array of contractile units known as sarcomeres (Fig. 3). Each sarcomere is situated between two Z-lines, transverse structures that provide structural stability to the sarcomere. The sarcomere contains two types of contractile myofilaments: thin filament actin and thick filament myosin. The actin filament is attached to the Z-line and extends toward the M-line, another transverse structure at the center of the sarcomere. This myofilament is made up of two filamentous actin strands that are tightly bound to two regulatory proteins, troponin and tropomyosin. On the other hand, the thick filament myosin consists of woven myosin molecules and is anchored to the M-line and extends toward the Z-lines. The overlapping of the thick and thin filaments within the sarcomere creates dark and light bands, giving the myofibrils a striated appearance. The dark region in the middle of the sarcomere is known as the A-band and spans the length of the myosin filament. Within this band is an area where the thick and thin filaments overlap and another that only contains thick filaments. The latter is known as the H-zone, which is bisected by the M-line. The light I-band is composed of actin from the adjacent half of neighboring sarcomeres.
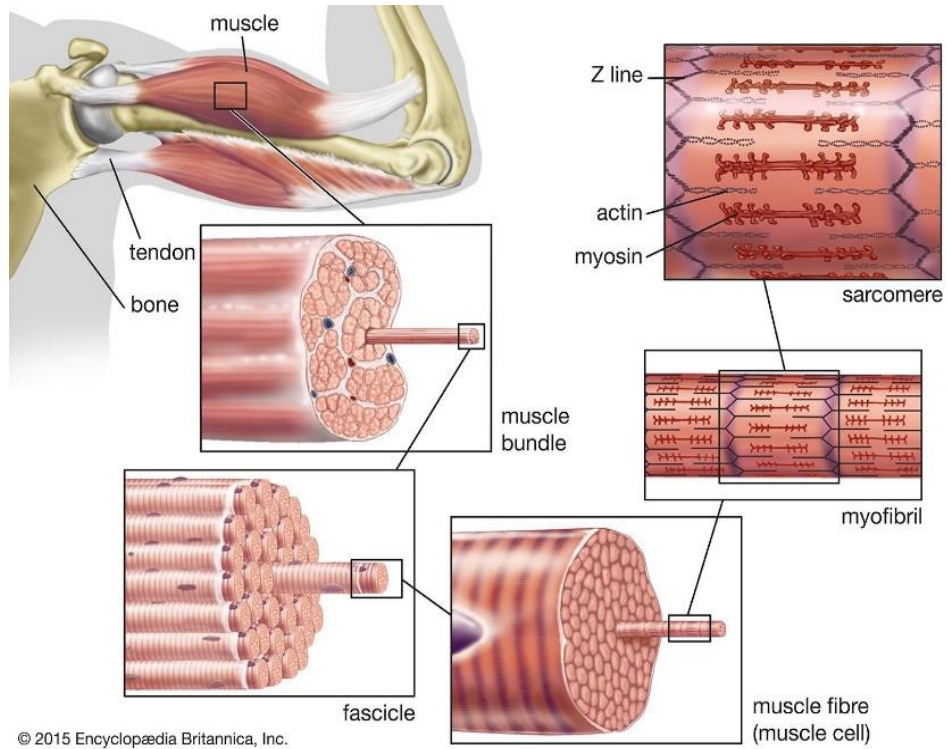
Fig. 2. The general organization of skeletal muscle, with permission form of Encyclopedia Britannica, Inc.
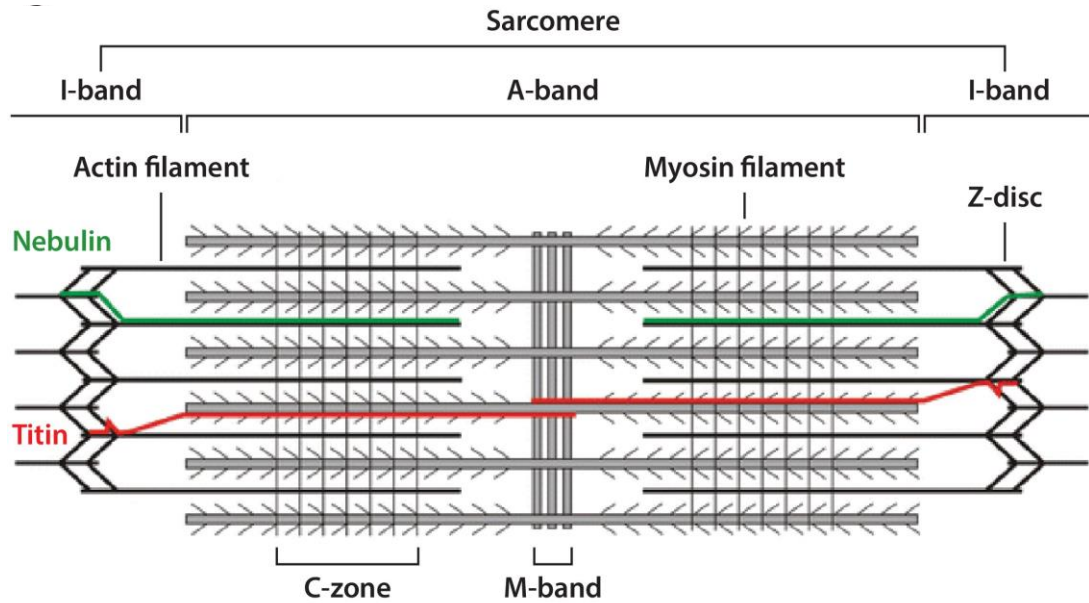
Fig. 3. Schematic representation of the sarcomere (Luther, 2009).

2.2. The Transformation of Muscle to Meat

The conversion of living muscle to consumable meat is a process that involves several physical and biochemical changes that take place after an animal's death. These changes are triggered by the sudden drop in oxygen delivery to the muscle and the subsequent shift to anaerobic metabolism. Under anaerobic metabolism, glycogen is metabolized through glycogenolysis (glycogen degradation) and glycolysis for the purpose of ATP production. The hydrolysis of ATP in postmortem muscle by muscle ATPases, yields H^+ that accumulate in the muscle resulting in its acidification (Hamm, 1977). This results in a gradual decline in muscle pH from ~ 7.2 to an ultimate pH of 5.5-5.7 in most meat species. As time progresses postmortem, the muscle's ability to create ATP diminishes, leading to a gradual decline in cellular ATP levels and, ultimately, complete depletion. In the absence of ATP, myosin binds irreversibly to actin, which increases muscle stiffness (rigor mortis). While rigor mortis is significant, in this literature review, we confine our focus to postmortem metabolism and pH decline and their relationship to meat quality development.

2.3. Postmortem Metabolism

The postmortem decline in muscle pH, resulting from postmortem anaerobic metabolism, is a key change dictating end-product quality. The rate and extent of postmortem pH decline have significant impacts on several fresh meat characteristics, including textural properties, color, flavor, and WHC. Thus, understanding factors controlling postmortem pH decline is essential to optimize meat quality.

The muscle cells continue to produce ATP during the first 24 h postmortem in a futile effort to maintain cellular homeostasis. Three metabolic pathways may function postmortem: the phosphagen system, anaerobic glycolysis, and mitochondrial oxidative

phosphorylation. The contribution of each of these systems will be discussed separately.

2.3.1. The phosphagen system

The phosphagen system is an energy-producing pathway that maintains ATP homeostasis during the early postmortem period. This metabolic system comprises three reactions that are cartelized by creatine kinase, adenylate kinase, and AMP deaminase. Phosphocreatine, a high-energy molecule found mainly in skeletal muscle, is broken down to creatine, inorganic phosphate, and energy in a reaction catalyzed by creatine kinase. This reaction supplies energy and inorganic phosphate to convert ADP to ATP (phosphocreatine + ADP + H^+ ↔ creatine + ATP). Once phosphocreatine is depleted, ADP starts to accumulate in postmortem muscle (Bendall, 1979). This activates the enzyme adenylate kinase, which converts two molecules of ADP to an ATP and an AMP. Subsequently, AMP is deaminated to inosine monophosphate (IMP) by the enzyme AMP deaminase. This reaction is important to shift the equilibrium of the adenylate kinase reaction to the right (ATP formation). However, deamination of AMP decreases the adenine nucleotide pool (ATP, ADP, and AMP), as IMP cannot be converted back to AMP in postmortem muscle. The phosphagen system is capable of supplying ATP for a brief period (a few minutes) before anaerobic glycolysis is triggered.

2.3.2. Glycogenolysis and glycolysis

Under postmortem anaerobic conditions, the primary pathways that maintain cellular ATP concentrations are glycogenolysis and glycolysis (England, Matarneh, Scheffler, & Gerrard, 2017). Glycogen is a complex glucose polymer stored in skeletal muscle and the major energy substrate postmortem. Glycogen phosphorylase and glycogen debranching enzymes break down glycogen's α-1,4- and α-1,6-glycosidic bonds, respectively,

producing glucose-1-phosphate and glucose. Glucose 1-phosphate is then converted to G6P by the enzyme phosphoglucomutase and consequently enters glycolysis (Fig. 1). G6P is metabolized through glycolysis to ultimately produce 2 pyruvates, 2 H_2O, 2 NADH, 3 ATP, and a H^+. In the absence of oxygen, pyruvate is converted to lactate by lactate dehydrogenase (Pyruvate + NADH + H^+ ↔ Lactate + NAD^+). The conversion of NADH to NAD^+ through this reaction is essential to the continuation of glycolysis in postmortem muscle, as NAD^+ is required for the glyceraldehyde 3-phosphate dehydrogenase (GAPDH) reaction of glycolysis. It is important to note that lactate accumulation is not responsible for the decline in postmortem muscle pH. Instead, the hydrolysis of ATP by muscle ATPases yields H^+ that accumulate in postmortem muscle due to the lack of circulation (Robergs, Ghiavand, & Parker, 2004). In living animals, the pH of the muscle is around 7.2; however, after harvest, it gradually drops to an ultimate pH of 5.5-5.7 (Fig. 4). For proper meat quality development, pH decline should follow a "normal" pattern; otherwise, adverse effects will develop (Scheffler & Gerrard, 2007).
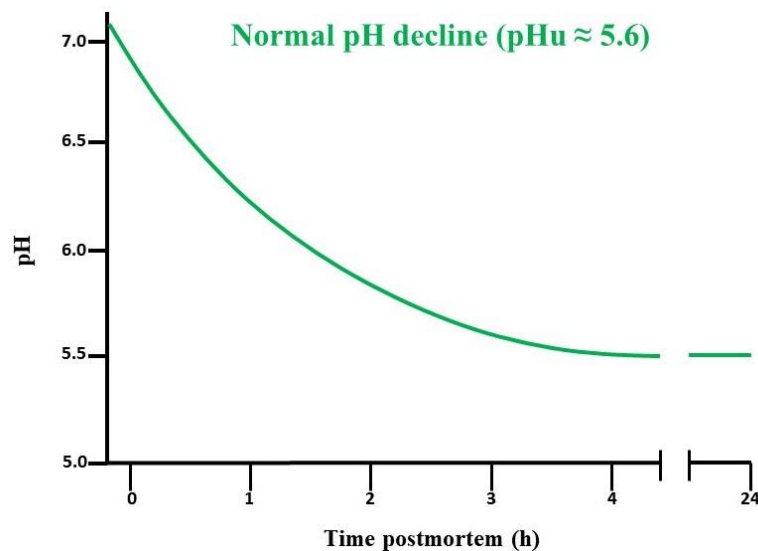
Fig. 4. A typical pH decline pattern in porcine *longissimus* muscle.

2.3.3. Mitochondrial oxidative phosphorylation

Mitochondria are the primary energy providers in muscle cells by means of cellular respiration. These organelles consist of two membranes, inner and outer. Between the two mitochondrial membranes is the intermembrane space, while the matrix is the aqueous compartment bounded by the inner membrane. Mitochondrial respiration begins with transporting substrates such as pyruvate and fatty acids into the matrix to be converted to acetyl-CoA. Acetyl-CoA is then completely oxidized by a series of reactions collectively known as the tricarboxylic acid (TCA) cycle (acetyl-CoA + 3NAD$^+$ + FAD + ADP + P$_i$ → COA + 2CO$_2$ + 3NADH + 3H$^+$ + FADH$_2$ + ATP). FADH$_2$ and NADH donate their electrons to the electron transport chain (ETC), a series of four protein complexes (complex I, II, II, and IV) embedded in the inner mitochondrial membrane, where the electrons travel through the complexes and eventually back to the matrix to bind with oxygen and H$^+$ to produce water. As electrons move through the ETC, their energy is harvested and used to pump protons from the matrix to the intermembrane space, creating an electrochemical gradient (proton motive force). These protons move back to the matrix down their electrochemical gradient through ATP synthase (complex V), and their energy is used to generate ATP.

Mitochondrial ETC loses functionality in an anoxic environment. Thus, it is generally believed that mitochondria are no longer relevant to postmortem metabolism. However, this is not entirely true according to recent research investigating mitochondrial functionality in postmortem muscle (England, Matarneh, Scheffler, Wachet, & Gerrard, 2014; Matarneh, *et al*., 2017; Matarneh, Yen, Bodmer, Kadi, & Gerrard, 2021). For

instance, England *et al.* (2018) found that oxygen consumption occurs gradually within the first two hours postmortem, indicating that residual mitochondrial respiration takes place in postmortem muscle. In a more recent study, Matarneh *et al.* (2021) reported that mitochondria are capable of metabolizing pyruvate in an *in vitro* model that mimics postmortem metabolism, but at reduced levels. Mitochondria have also been shown to increase the rate of ATP hydrolysis *in vitro*, which, in turn, increased the rate and extent of anaerobic metabolism and pH decline (Matarneh, Berine, Silva, Shi, & Gerrard, 2018). Collectively, these studies suggest that mitochondria play a more prominent role than previously thought. Yet, further research is warranted to precisely define the role mitochondria play in postmortem metabolism.

2.4. Postmortem pH Decline and Meat Quality

The rate and extent of pH decline in postmortem muscle strongly influence the quality of the resulting meat. Any deviation from the normal pH decline pattern (Fig. 4) in muscle postmortem can have an adverse effect on meat color (Swatland, 2008), texture (Beltrán *et al.*, 1997), flavor, WHC, and shelf life (Bouton, Harris, & Shorthose, 1971).

2.4.1 *Water-holding capacity*

Water-holding capacity is defined as meat's ability to hold water under the application of external force, such as cutting, grinding, pressing, or cooking (Hamm, 1986). It is one of the most important attributes of fresh meat that determines its economic and quality value. Essentially, water loss can lead to a decrease in meat yield and negatively affect its color, texture, and juiciness.

Water is a dipolar molecule that is attracted to electrically charged groups like proteins. The ultimate pH of meat controls the ionization state of muscle proteins and, thus,

WHC (den Hertog-Meischke, van Laack, & Smulders, 1997). A pH of 5.1-5.2 is the average isoelectric point (pI) of muscle protein (Matarneh, England, Scheffler, & Gerrard, 2017), at which the net charge is zero. At pI, there are minimal charges available for water to interact with, which substantially impairs the WHC of the meat. When meat's pH falls away from the pI (either higher or lower), the net charge on muscle protein increases and, subsequently, the ability to hold water. Further, the increase in the net charge causes muscle structures to push away from each other (repulsion), thereby increasing the space for water to occupy (i.e., steric effect). The rate of postmortem pH declines can also impact the WHC of meat. When the pH drops rapidly while the carcass is still warm, as in PSE, it causes extensive denaturation of proteins, which in turn diminishes their ability to retain water. (Molette *et al*., 2003).

2.4.2   Color

Meat color significantly affects consumer purchasing decisions, with consumers being less likely to buy meat that is lighter or darker than the typical color, causing economic losses for the industry (Gao *et al*., 2013). Observed meat color is determined by how light interacts with its surface (reflection, absorption, or scattering), but the most critical factor is the reflection of light as seen by the eye. The reflection is affected by fluid distribution within the meat (intra- vs. extracellular) (Hughes *et al*., 2014). A lighter appearance results from increased fluid in the extracellular space due to low water WHC, while the opposite is true when WHC is high (Purslow, 2020).

The color of meat is intimately tied to the extent of postmortem pH decline. Meat with a low ultimate pH (pH < 5.4) tends to have lighter color compared to meat with normal ultimate pH (~ 5.6), whereas meat with a high ultimate pH (pH > 6.0) appears darker. The

effect of ultimate pH on meat color is mainly induced through modulating WHC. Impaired WHC associated with low ultimate pH increases water content within the extracellular space, which increases light reflectance and scattering on the meat surface, making it appear lighter. This also results in more water loss from the meat through purging and dripping, causing myoglobin, the water-soluble protein that gives meat its color, to be lost and exacerbating the problem (Gao *et al*., 2013). Conversely, meat with a high ultimate pH has increased WHC, less water in the extracellular space, less light scattering, and less myoglobin loss, resulting in a darker color. Not just the extent of pH decline affects meat color, but also the rate of pH decline. Hastened pH decline increases protein denaturation, leading to reduced WHC and lighter product.

2.4.3   Texture

Texture is deemed the most crucial aspect of the eating experience among all meat quality traits. (Miller, Carr, Ramsey, Crockett, & Hoover, 2001; Van Wezemael, Desmet, Veland, & Verbeke, 2014). Similar to color, meat texture is affected by the rate and extent of pH decline through modifying WHC. Meat with low ultimate pH exhibits increased water loss and shrunk muscle fibers, which makes it abnormally soft and "mushy" upon cooking (Solomon, Van Laack, & Eastridge, 1998). On the contrary, a high ultimate pH and WHC result in larger muscle fibers and firmer meat (Klont, Brocks, & Eikelenboom, 1998). A rapid drop of postmortem muscle also negatively affects pork texture, much like a low ultimate pH.

2.5. Meat Defects

There are several major defects that can impact the quality of meat, including dark, firm, and dry (DFD), pale, soft, and exudative (PSE), and acid meat (Fig. 5). These defects

can arise due to genetic mutations or antemortem stress factors such as poor handling and severe environmental conditions. The impact of these defects on both meat quality and consumer acceptance is substantial, making it imperative to closely monitor and control them to ensure the production of high-quality meat. The following three sections will discuss these defects.

2.5.1. *Dark, firm, and dry*

DFD results when the ultimate pH halts at a higher than normal value (pH > 6), resulting in meat that has an abnormally dark color, firm texture, and dry feel. The occurrence of DFD is prevalent in beef and is primarily caused by chronic antemortem stress that leads to muscle glycogen depletion, which, in turn, causes early termination of glycolysis (Matarneh, Silva, *et al.*, 2021). Antemortem stressors such as mixing unfamiliar animals, inclement weather conditions, and improper handling trigger the release of catecholamines (epinephrine and norepinephrine) that stimulate glycogen breakdown. The high ultimate pH of DFD meat is associated with increased WHC, which induces DFD characteristics. It is important to point out that DFD meat is prone to bacterial spoilage and loss of profit as consumers are put off by the darker color (Newton & Gill, 1981).
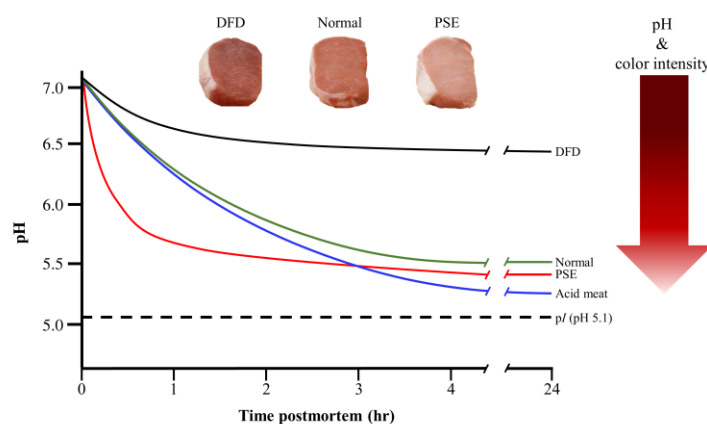
Fig.5. The influence of the rate and extent of postmortem pH decline on meat quality.

2.5.2. Acid meat

Acid meat is a defect that occurs mainly in pork and is identified as pale coloration of the meat. This defect is associated with an ultimate pH that is below the normal ultimate pH range (pH < 5.4). The impaired ability to retain water due to the low pH is the main reason for the inferior quality of acid meat. The occurrence of acid meat is typically attributed to the AMPKγ3^{R200Q} mutation, which is most notably found in Hampshire-bred pigs (Scheffler, Parks, & Gerrard, 2011). Pigs carrying this mutation deposit up to 100% more glycogen than wild-type pigs. As such, it has been suggested that the low ultimate pH of meat from these pigs is a function of their elevated muscle glycogen. However, recent research indicates that increased glycolytic flux in the postmortem muscle of these mutant pigs is the reason for their lower ultimate pH pork (Matarneh *et al*., 2017).

2.5.3. Pale, soft, and exudative

PSE is a meat defect commonly found in pork and poultry that results from a hastened postmortem pH decline while the carcass is still warm (39-40 °C). The combined effect of low pH and elevated temperature causes excessive protein denaturation, a decrease in proteins' ability to bind water, and the loss of muscle structural integrity, causing the meat to be pale in color and soft in texture. It is worth mentioning that the ultimate pH of PSE meat often falls within the normal range (pH 5.5-5.7).

A major reason for PSE conditions is the exposure to acute stressors just before harvest. Unlike DFD, this short-term stress does not deplete muscle glycogen but improves the rate of postmortem glycogenolysis and glycolysis, thereby causing a fast decline in muscle pH. The release of catecholamines during stressful situations triggers a signaling cascade designed to meet the energy requirement of the stressor. Specifically, epinephrine

stimulates the conversion of glycogen phosphorylase *b* (the less active form) to glycogen phosphorylase *a* (the more active form), increasing glycogen degradation rate.

The occurrence of severe PSE cases is associated with a condition known as Porcine Stress Syndrome. This syndrome is predominantly induced by a genetic mutation known as halothane mutation (HAL), a single base substitution mutation (C1843 to T) in the gene that encodes the RYR1, the calcium-releasing channel on the SR (Fujii *et al*., 1991). At the protein level, this mutation results in the substitutes of arginine 615 with cysteine, leading to the release of approximately twice the amount of Ca^{2+} into the cytosol (Mickelson & Louis, 1996). In addition, this mutation impairs RYR1 capacity to uptake Ca^{2+} (Küchenmeister, Kuhn, Weagner, Nürnberg, & Ender, 1999). Increased cytosolic calcium levels initiate muscle contraction, which increases the rate of ATP hydrolysis by myosin ATPase. In addition, high levels of intracellular calcium stimulate the SR calcium pump ATPase to sequester calcium into the SR, which further increases the rate of ATP hydrolysis. Recall, the primary source of H^+ in postmortem muscle is the hydrolysis of ATP, so accelerating the rate of ATP hydrolysis hastens muscle acidification. Scopes (1974) demonstrated that the rate of postmortem ATP hydrolysis dictates the rate of anaerobic metabolism and pH decline. He also indicated that the rate of ATP hydrolysis determines the flux through glycolysis. Essentially, increasing the rate of ATP hydrolysis accelerates glycolysis to cope with the extra energy demands. For instance, the activity of pyruvate kinase, one of the rate-limiting enzymes of glycolysis, was found to be four-fold higher in PSE muscle compared to normal muscle (Schwägele, Haschke, Honikel, & Krauss, 1996).

In addition to improving the rate of ATP hydrolysis, increased cytosolic calcium

improves glycogenolysis through activating phosphorylase kinase, the enzyme that phosphorylates and activates glycogen phosphorylase, thereby contributing to a faster metabolism. While eliminating the HAL mutation from pig breeds has reduced the prevalence of PSE, this defect is still a significant concern to the pork and poultry industries (Petracci, Bianchi, & Cavani, 2009).

2.6. Pyruvate Metabolism

Pyruvate is an important metabolite that serves as a "hub" for multiple energy pathways. In addition, pyruvate is a precursor for many amino acids, sugars, and fatty acids. However, under postmortem low energy charge, pyruvate is utilized for the sole purpose of energy production. There are four main enzymes that utilize pyruvate in the cell: pyruvate dehydrogenase (PDH), pyruvate carboxylase (PC), lactate dehydrogenase (LDH), and malic enzyme (ME).

2.6.1. *Pyruvate dehydrogenase*

The pyruvate dehydrogenase complex utilizes pyruvate to generate energy or to fulfill biosynthetic purposes (Gray, Tompkins, & Taylor, 2014). PDH is located in the inner mitochondrial membrane facing toward the matrix (Patel & Korotchkina, 2006). Pyruvate's entry across the outer mitochondrial membrane is facilitated by a non-specific voltage-dependent anion channel (McCommis & Finck, 2015) and through the inner membrane by MPC1 and MPC2 pyruvate carriers (Bricker *et al*., 2012; Sheeran, Angerosa, Liaw, Cheung, & Pepe, 2019). Once in the matrix, PDH converts pyruvate to acetyl-CoA, a two-carbon compound. Acetyl-CoA has multiple possible anabolic applications, including lipid synthesis, cholesterol formation, and acetylcholine generation, or it can enter the TCA cycle. In the latter case, acetyl-CoA is condensed with oxaloacetate to citrate (six-carbon

compound) by citrate synthase. Citrate is then metabolized through the TCA cycle to produce 3 NADH, ATP, and $FADH_2$. The NADH and $FADH_2$ enter the ETC to produce more ATP. This process takes place under aerobic conditions and shuts down in the absence of oxygen. Hence, the involvement of mitochondria in postmortem metabolism has been greatly disregarded. However, recent *in vitro* research found that mitochondria can metabolize a portion of glycolytic pyruvate, albeit at reduced levels (Matarneh, Yen, Bodmer, Kadi, & Gerrard, 2021).

2.6.2. *Pyruvate carboxylase*

Pyruvate carboxylase is a cytosolic enzyme that catalyzes the conversion of pyruvate to oxaloacetate. PC has three domains: biotin carboxylase domain, carboxyl transferase domain, and a biotin carboxyl carrier protein domain (Adina-Zada, Zeczycki, & Attwood, 2012). In the cytosol, PC converts pyruvate to oxaloacetate. However, oxaloacetate cannot enter the mitochondria due to the lack of a transport protein on the mitochondrial inner membrane. To be transported into the mitochondrial matrix, oxaloacetate is first converted to malate in a reaction catalyzed by cytosolic malate dehydrogenase (Haslam & Krebs, 1968). Malate then enters the mitochondria via the malate-aspartate shuttle (Bremer & Davis, 1975). Once inside, malate is converted back to oxaloacetate by mitochondrial malate dehydrogenase.

2.6.3. *Malic enzymes*

Malic enzyme is another enzyme found in the cytosol that utilizes pyruvate in an NADPH-dependent reaction. This enzyme converts pyruvate to malate by reductive carboxylation (Heart *et al*., 2009; Skorkowski, 1988). As explained above, malate can then be shuttled into the mitochondria by the malate-aspartate shuttle.

2.6.4.   Lactate dehydrogenase

Lactate dehydrogenase is a tetrameric enzyme that belongs to the 2-hydroxy acid oxidoreductase family (Jafary, Ganjalikhany, Moradi, Hemati, & Jafari, 2019). This enzyme catalyzes the reversible reduction of pyruvate to lactate, a reaction that can occur in aerobic and anaerobic environments. Converting pyruvate to lactate requires the oxidation of NADH to NAD$^+$; LDH removes a hydride ion from the NADH, restoring it to NAD$^+$, and then attaches the hydride ion to the C$_2$ carbon of the pyruvate to produce lactate (Valvona, Fillmore, Nunn, Pilkington, 2016). The LDH reaction is important for the continuity of postmortem glycolysis, as the NAD$^+$ produced through this reaction is required for the GAPDH reaction of glycolysis.

2.7. Mass Spectrometry of Metabolites

To study the complex molecular makeup of biological systems, the use of mass spectrometry is employed. Mass spectrometry is a powerful analytical technique that takes a sample and ionizes it into a stream of charged particles, where they will be separated based on their mass-to-charge ratio (El-Aneed, Cohen, & Bunoub, 2009). This separation of masses results in information on the molecular composition of the sample. It also has the ability to detect a wide range of metabolites, including those with polar, non-polar, and ionizable function groups (Dettmer, Aronov, & Hammock, 2007). Additionally, mass spectrometry also contains several different methods that can be used for metabolomics, each with its own weakness and strengths, with the method used depending on the sample type and specific question being asked.

The complexity and connection of the different metabolic pathways in muscle cells make it difficult to understand cellular metabolism globally. After years of development,

the use of metabolic flux analysis (MFA) has become the method of choice to investigate metabolic pathways and their interactions. MFA can be utilized to track the fates of carbon compounds through a targeted system. Isotope-labeled carbon substrates are added to the cell population of interest until the substrate is distributed throughout the system (Bremer & Davis, 1975). These isotopes allow researchers to tract the pathway in which certain carbon substrates are utilized. This provides us the ability to further our understanding of how mitochondria are involved in postmortem metabolism.

2.8. Summary

A complete understanding of the complex system of postmortem muscle metabolism has yet to be achieved, as some information is missing or not fully understood. Even the currently held understanding is being revised. For example, it was previously thought that mitochondria are dysfunctional after harvest, but new evidence shows that they retain the ability to uptake pyruvate, even without oxygen. Furthermore, an impact on glycolysis by reducing the substrate available for glycolysis could occur. These insights about mitochondria could lead to a new understanding of what happens in skeletal muscle postmortem. Therefore, we hypothesize that mitochondria modulate the rate of postmortem glycolysis and pH decline by consuming a portion of glycolytic pyruvate. Thus, by inhibiting the mitochondrial ability to consume glycolytic pyruvate, we can determine if they affect the rate of postmortem glycolysis.

3. MATERIALS AND METHODS

3.1. Muscle Sample Collection

Ten male market-weight pigs raised under the same conditions were humanely harvested at the Utah State University Animal Harvest Facility following USDA inspection procedures. Within 5 min postmortem, a sample from the *longissimus lumborum* (*LL*) muscle was collected from one side of each carcass, snap-frozen in liquid nitrogen, and stored at −80 °C to be used for the Scopes *in vitro* model.

3.2. *In vitro* Model and Experimental Design

The modified Scopes *in vitro* model was utilized to test our hypothesis. This *model* consists of a buffer containing all metabolites required for glycolysis and powdered pre-rigor muscle that provides glycolytic and mitochondrial enzymes (England, Matarneh, Scheffler, Wachet, & Gerrard, 2014). Frozen *LL* muscle samples were pulverized under liquid nitrogen, and four subsamples (~1 g each) were collected from each sample in 15-ml centrifuge tubes. Pulverized muscle samples were homogenized at a 1:10 ratio in a reaction buffer containing 10 mM Na_2HPO_4, 30 mM creatine, 25 mM carnosine, 10 mM Na-acetate, 60 mM KCl, 5 mM $MgCl_2$, 40 mM glycogen, 5 mM ATP, 0.5 mM ADP, and 0.5 mM NAD^+ (pH 7.4). Immediately after homogenization, one tube received CPI-613 (a pyruvate dehydrogenase [PDH] inhibitor; final concentration, 400 µM), the second tube received 1.5 U/ml Avidin (a pyruvate carboxylase [PC] inhibitor), the third tube received CPI-613 + Avidin (same concentrations as above), and the fourth tube received diluent (control). Reaction vessels were stored at 25 °C, and aliquots were removed at 0, 60, 120, 240, and 1440 min to determine pH and glycolytic metabolites.

The same experimental design detailed above was utilized in a subsequent experiment but with some modifications. Two treatments, control and 400 µM CPI-613, were tested instead of four treatments. Additionally, a ^{13}C-labeled glucose tracer ([$^{13}C_6$]glucose) was used instead of glycogen, and 0.25 U/ml hexokinase was included in the *in vitro* model to promote the conversion of glucose to glucose 6-phosphate.

3.3. Mass Spectrometry of Metabolites

[13]C-Enrichment of glycolytic and TCA cycle metabolites was analyzed by GC–MS followed by ^{13}C-mass isotopomer distribution analysis (Des Rosiers *et al*., 1995; Fernandez *et al*., 1996). Briefly, aliquots of tissue homogenate from the second *in vitro* experiment were mixed with 1 M perchloric acid, incubated on ice for 20 min, centrifuged at 17,000 $\times g$ for 5 min, and the supernatant was neutralized with KOH. Then, sulfosalicylic acid was added to achieve a final concentration of 10%, and the samples were centrifuged at 3000 $\times g$ for 5 min. The supernatant was transferred to a new tube, and 5 mM of hydroxylamine-hydrochloride was added. Next, the pH was adjusted to < 2, and the solution was saturated with NaCl to precipitate sulfosalicylic acid. The supernatant was extracted with ethyl acetate, centrifuged at 2000 $\times g$ for 5 min, and the organic phase was collected. Samples were dried under nitrogen gas to form the tertiary-butyldimethylsilyl (tBDMS) derivatives. tBDMS derivatives were separated by GC on a fused silica capillary column (Agilent, Palo Alto, CA, USA) as previously described (El-Kadi, Baldwin, McLeod, Sunny, & Bequette, 2009). Ions with mass-to-charge (*m/z*) were monitored under single ion monitoring. Enrichments were expressed as tracer-tracee ratios in mole percent excess.

3.4. pH Determination

Aliquots for pH analysis were mixed with a buffer containing 25 mM iodoacetate and

750 mM KCl (pH 7.0) at 4:1 ratio (Bendall, 1979). Samples were then centrifuged at 17,000 $\times g$ for 5 min at room temperature, equilibrated to 25 °C in a dry heating block, and measured directly using an Orion Ross Ultra pH electrode attached to an Orion Star A214 pH/ISE benchtop meter (Thermo Scientific, Pittsburgh, PA, USA). Standard buffer solutions with pH values of 4, 7, and 10 were used to calibrate the pH electrode daily.

3.5. Glycolytic Metabolite Determination

Glycogen samples were prepared by mixing 300 µl of tissue homogenate with the same volume of 2.5 M HCl. The resulting mixture was incubated for 2 h at 90 °C, centrifuged at 17,000 $\times g$ for 5 min, and the supernatant was neutralized with 1.25 M KOH. Glucose, glucose 6-phosphate, and lactate were evaluated on a different aliquot treated with the same volume of 1 M perchloric acid. Samples were placed on ice for 20 min, centrifuged at 17,000 $\times g$ for 5 min, and supernatants were neutralized with 0.5 M KOH (Bergmeyer, 1984). Concentrations of all metabolites were determined spectrophotometrically at 340 nm with enzymatic methods modified for a 96-well microplate (Hammelman $et\ al.$, 2003).

3.6. Pyruvate Dehydrogenase Activity

PDH activity was determined using the PDH Activity Assay Kit according to the manufacturer's protocol (MAK183; Sigma-Aldrich, Visalia, CA, USA). The assay was carried out in the presence of 0, 50, 100, 200, 400, 800, or 1600 µM CPI-613. The increase in absorbance due to the reduction of NAD^+ to NADH was measured spectrophotometrically at 340 nm every 1 min for 10 min using a plate reader (Epoch 2, BioTek, Winooski, VT, USA). Activity values were reported as nmol NADH/min/mg tissue.

3.7. Pyruvate Carboxylase Activity

PC activity was determined spectrophotometrically using the Pyruvate Carboxylase Microplate Assay Kit in accordance with the manufacturer's directions (orb759229; Biorbyt, Cambridge, UK). The assay was carried out in 96-well microplates in the presence of 0, 0.5, 1.0, 1.5, 3.0, 9.0, or 12.0 U/ml Avidin, and the change in absorbance was measured at 340 nm. PC activity was expressed as nmol NADH/min/mg tissue.

3.8. Glycogen Phosphorylase Activity

Glycogen phosphorylase a (GPa) and total (GPt) activities were analyzed following the procedures outlined by Bergmeyer (1984). Briefly, powdered *LL* muscle tissue was homogenized at a 1:20 ratio in an ice-cold 100 mM K_2HPO_4 solution (pH 7.4) using a Polytron homogenizer (Polytron PT 2500 E, Kinematica AG, Switzerland). An aliquot of the tissue homogenate was then added to a reaction buffer containing 50 mM K_2HPO_4, 2 mg/ml glycogen, 1.3 mM $MgCl_2$, 0.1 mM EDTA, 0.5 mM NADP, 200 mM MES (pH 6.8), 1 U/ml phosphoglucomutase and 1 U/ml glucose 6-phosphate dehydrogenase with or without 400 µM CPI-613 to measure GPa activity. The reaction mixture was immediately transferred in duplicate to a 96-well microplate, where kinetic measurements were conducted at 340 nm using a spectrophotometer. GPt activity was determined utilizing the same reaction buffer supplemented with 1.75 mM AMP. GPa and GPt results were reported as $\mu mol\ NADH * min^{-1} * g\ tissue^{-1}$.

3.9. Phosphofructokinase Activity

Determination of Phosphofructokinase (PFK) activity followed a modified procedure described by (Trivedi, 1966). Powdered *LL* samples were homogenized at a 1:20 ratio in an ice-cold buffer containing 0.1M K_2HPO_4 (pH 7.4) for 5×10 s bursts. Muscle

homogenates were aliquoted into tubes with a reaction buffer consisting of 120 mM MES (pH 7.4), 3.2 mM MgSO$_4$, 1 mM NADH, 3 mM fructose 6-phosphate, 2 U/ml triosephosphate isomerase, 1 U/ml glycerol-3-phosphate dehydrogenase, and 1 U/ml aldolase in the presence or absence of 400 µM CPI-613. The change in absorbance due to the oxidation of NADH to NAD$^+$ was evaluated spectrophotometrically at 340 nm for 7 min at 1 min intervals. The results were reported as µmol NADH $*$ min^{-1} $*$ g tissue^{-1}.

3.10. Pyruvate Kinase Activity Assay

The method described by Feliu *et al.* (1976) was utilized to determine pyruvate kinase (PK) activity. In brief, *LL* muscle tissue was homogenized in an ice-cold buffer containing 100 mM K$_2$HPO$_4$ (pH 7.4) at a 1:20 ratio. The resulting mixture was combined with a buffer containing 120 mM MES (pH 6.5), 100 mM KCl, 10 mM MgCl$_2$, 1.25 mM ADP, 1 mM NADH, 0.5 mM phosphoenolpyruvate (PEP), and 2 U/ml lactate dehydrogenase with or without 400 µM CPI-613. The reduction in absorbance due to the conversion of NADH to NAD$^+$ was measured at 340 nm for 7 min at 1 min intervals using a spectrophotometer. PK activity was reported as µmol NADH $*$ min^{-1} $*$ g tissue^{-1}.

3.11. Statistical Analysis

Obtained data were analyzed using the mixed model of SAS (SAS Institute Inc., Cary, NC, USA) for repeated measures. The statistical model included the main effects of treatment, time, and their interactions, and the random effect of the reaction tube. Differences were evaluated using a Tukey-Kramer post hoc test, with $P \leq 0.05$ considered statistically significant.

4. RESULTS AND DISCUSSION

Pyruvate is an essential metabolite that serves as a "hub" for various energy pathways and a precursor for several amino acids and TCA cycle intermediates. However, under postmortem low energy charge, pyruvate is utilized for the sole purpose of energy production. Four main enzymes utilize pyruvate in muscle cells: PDH, PC, malic enzyme, and lactate dehydrogenase (LDH). While the latter is traditionally recognized as the primary enzyme responsible for utilizing pyruvate in postmortem muscle, new observations suggest that pyruvate can be partially utilized or recycled in the mitochondria under anoxic conditions (Matarneh, Yen, Bodmer, Kadi, & Gerrard, 2021), likely facilitated by the action of the former three enzymes.

PDH is a mitochondrial enzyme that catalyzes the conversion of pyruvate to acetyl-CoA, which is then utilized in the TCA cycle. In contrast, PC and malic enzyme are cytosolic enzymes that catalyze the conversion of pyruvate to oxaloacetate and malate, respectively. These two metabolites are then transported into the mitochondria for further metabolism. In the current study, PDH and PC were inhibited using CPI-613 and Avidin, respectively. However, we could not procure a specific inhibitor for malic enzyme at the beginning of the study; thus, malic enzyme was not inhibited. CPI-613, a stable analog of lipoic acid, inactivates PDH by activating lipoate-sensitive pyruvate dehydrogenase regulatory kinases, which phosphorylate and inactivate PDH (Alistar *et al*., 2017; Dörsam & Fahrer, 2016). On the other hand, Avidin is a glycoprotein found in chicken egg white that contains four biotin-binding sites (Attwood, Mayer, & Wallace, 1986). It inhibits PC by binding to its biotin prosthetic group, thus blocking the enzyme's active site (Johannssen, Attwood, Wallace, & Keech, 1983).

To test the inhibitory effect of CPI-613 on PDH, we evaluated muscle PDH activity in the presence of 7 different concentrations of CPI-613 (0, 50, 100, 200, 400, 800, 1600 µM). We used the 0 µM CPI-613 group as a reference point with 0% inhibition (100% activity), and the inhibitory effects of the other treatments were calculated comparatively. The obtained data indicate that CPI-613 effectively inhibited PDH activity ($P < 0.0001$, Fig. 6A). The inhibitory effect of CPI-613 on PDH generally increased with increasing CPI-613 concentration, but not statistically between 200-1600 µM. Similarly, PC activity was tested at 7 different levels of Avidin (0, 0.5, 1, 1.5, 3, 9, or 12 U/ml), and percent inhibition values were expressed comparatively to the 0 U/ml Avidin treatment. The inhibitory effect increased with increasing the concentration of Avidin from 0 to 1.5 U/mL and plateaued thereafter ($P < 0.0001$, Fig. 6B). These results led us to opt for a concentration of 400 µM CPI-613 and 1.5 U/ml Avidin for the *in vitro* experiments. These concentrations were selected because our data indicated that higher concentrations did not yield a greater inhibitory effect. The chosen concentrations of Avidin and CPI-613 provided ~ 60 and 70% inhibition for PDH and PC, receptively.
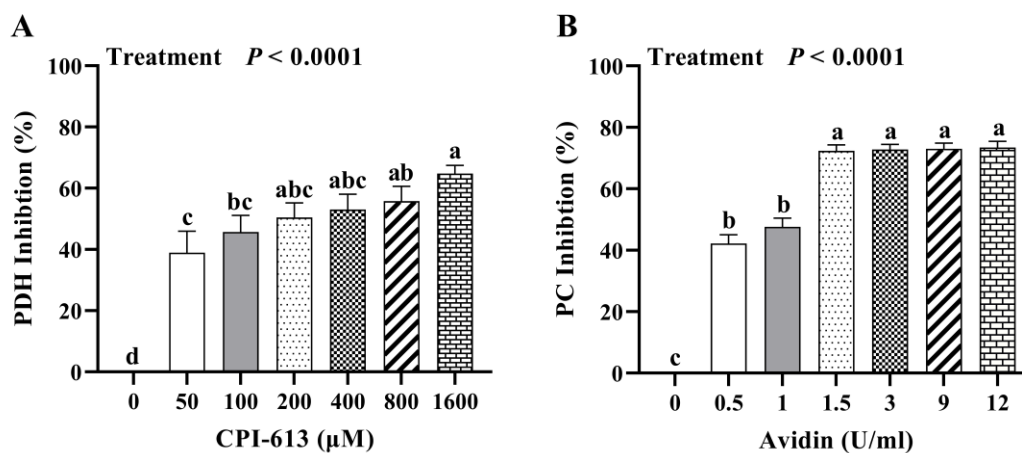
Fig. 6. Percent activity inhibition of pyruvate dehydrogenase (%; A) and pyruvate carboxylase (%; B). Data are LS means ± SE. [a,b,c]Means lacking a common letter differ ($P \leq 0.05$).

4.1. pH and Glycolytic Metabolites

A significant treatment × time interaction was detected for the *in vitro* system pH (P < 0.0001, Fig. 7). The pH values of all treatments were similar at 0 min (~ pH 6.9) and gradually decreased thereafter (P < 0.0001). Treatments containing CPI-613, with or without Avidin, lowered the pH at 60, 120, 240, and 1440 min compared to the control or Avidin treatments (P ≤ 0.03). No difference in pH was observed between Avidin and control at all time points (P = 0.94). These results indicate that inhibiting PDH increased the rate and extent of pH decline in the *in vitro* system, while inhibiting PC had no effect.

The concentration of glycogen, glucose, G6P, and lactate was also evaluated in this study to better understand the underlying mechanism behind the difference in pH between treatments (Fig. 8). Glycogen is the predominant energy substrate in postmortem muscle. The combined action of glycogen phosphorylase and glycogen debranching enzyme is required for the complete degradation of glycogen into glucose-1-phosphate and glucose (Calder & Geddes, 1990; Matarneh, Silva, Gerrard, 2021). There was a treatment × time interaction for glycogen concentration in the *in vitro* model (P < 0.0001, Fig. 8A). As expected, the glycogen content of all treatments declined over time (P < 0.0001). At 60, 120, and 240 min, the CPI-613 and CPI-613 + Avidin treatments had lower glycogen than the Avidin and control treatments (P ≤ 0.0003). Yet, all treatments had comparable glycogen contents at 1440 min.
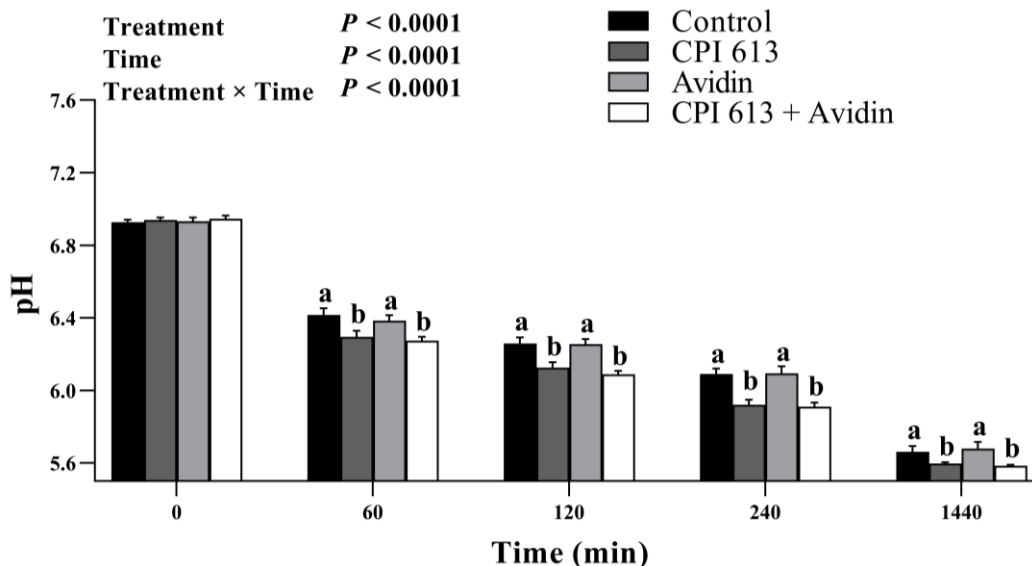
Fig. 7. Mean pH of the *in vitro* model. Data are LS means ± SE. [a,b]Means lacking a common letter differ within a time point ($P \leq 0.05$).

Glucose-1-phosphate produced via glycogenolysis is converted to G6P by the enzyme phosphoglucomutase. G6P is then metabolized through glycolysis to ultimately produce two pyruvate molecules. The increased glycogen degradation at 60, 120, and 240 min in the CPI-613-containing treatments resulted in greater G6P levels in those same treatments at those same time points ($P \leq 0.03$, Fig. 8B), whereas no variation in G6P was detected among treatments at 0 and 1440 min. A treatment × time interaction was also noted for the *in vitro* model glucose level ($P < 0.0001$, Fig. 8C). Glucose was greater in reaction vessels containing CPI-613 in the presence or absence of Avidin at 60 and 120 min compared to Avidin and control ($P \leq 0.05$). However, the glucose level in reaction vessels containing Avidin at 1440 min was greater than those containing CPI-613 with or without Avidin, but comparable to the control ($P = 0.01$).

Postmortem muscle's anoxic conditions prompt the conversion of pyruvate to lactate, while the hydrolysis of glycolytic ATP by muscle ATPases yields H^+. The absence of blood

circulation in postmortem muscle causes lactate and H^+ to accumulate, resulting in a pH decline. Because lactate and H^+ are produced in equal amounts, lactate is often used as a marker of the rate and extent of postmortem metabolism (Marcinek et al., 2010; Matarneh, Silva, Gerrard, 2021). Treatments differentially affected lactate levels over time (treatment × time, $P < 0.0001$, Fig. 8D). Greater lactate levels were observed in reaction vessels containing CPI-613, with or without Avidin, at 60 and 240 min when compared to the Avidin and control treatments ($P \leq 0.04$). At 120 min, the CPI-613 + Avidin treatment had greater lactate than the control, while Avidin and CPI-613 treatments were intermediate ($P = 0.008$). There was no difference in lactate concentration between the CPI-613 and Avidin treatments at 1440 min, but both had lower lactate than the CPI-613 + Avidin treatment and greater lactate than the control ($P = 0.03$).

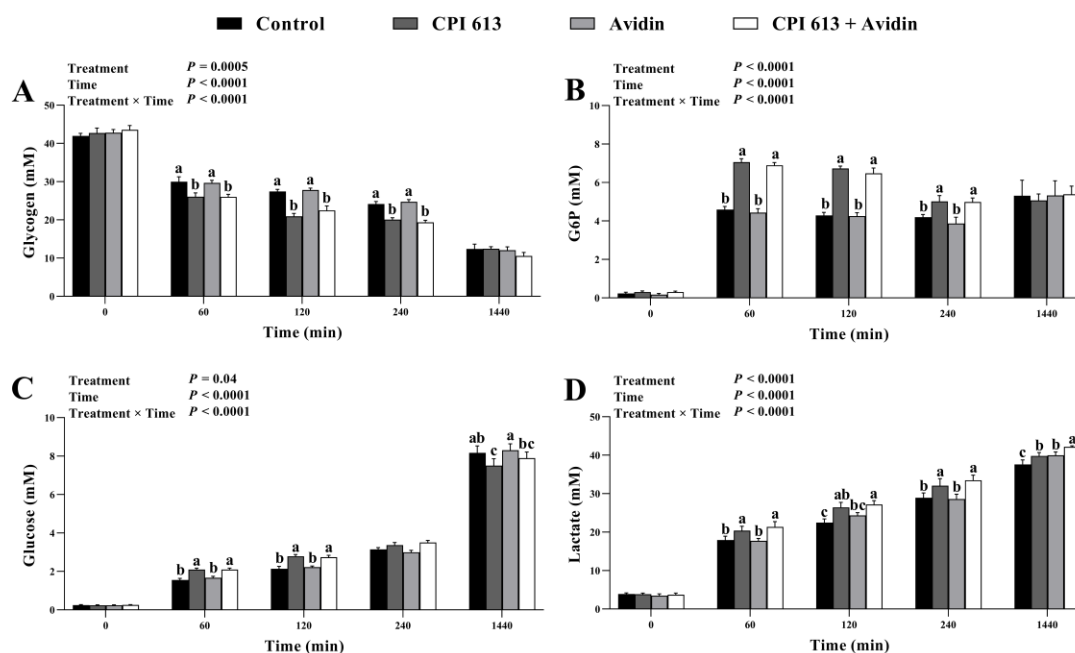**Fig. 8.** Mean glycolytic metabolite concentrations: glycogen (mM; A), glucose-6-phosphate (mM; B), glucose (mM; C), lactate (mM; D) of the *in vitro* model. Data are LS means ± SE. [a,b,c]Means lacking a common letter differ within a time point ($P \leq 0.05$).

We observed greater glycogen degradation and more G6P, glucose, and lactate accumulation in the CPI-613-containing treatments across most time points. These findings indicate that PDH inhibition increased the rate of glycogenolysis and glycolysis, which explains the increase in the rate of pH decline. Although there was no difference in glycogen concentration between treatments at 1440 min, a difference in lactate was detected, indicating an unequal glycolytic flux. When glycogen degradation is similar, a greater lactate concentration suggests greater flux through glycolysis, while lower lactate indicates a greater accumulation of glycolytic intermediates. Indeed, the control and Avidin treatments had greater glucose at 1440 min in comparison to the CPI-613 treatment. In contrast to PDH inhibition, inhibition of PC did not affect glycogenolysis or glycolysis. Using ^{13}C-labeled glucose tracer, (Kowalski *et al*., 2015) reported that > 95% of pyruvate enters the TCA cycle via PDH. This could account for the lack of effect of PC inhibition, given its minor contribution to pyruvate metabolism compared to PDH.

LDH catalyzes the conversion of pyruvate to lactate in postmortem muscle in a reaction involving the reduction of NADH to NAD^+. This is crucial because NAD^+ is necessary for the GAPDH reaction of glycolysis, allowing glycolysis to continue postmortem. Unlike LDH, the PDH reaction consumes NAD^+ and generates NADH. Considering the vital role of NAD^+ in glycolysis, we suggest that inhibiting PDH increases NAD^+ availability and supports greater levels of glycolysis and, subsequently, faster pH decline. In addition, preventing pyruvate consumption by PDH increases pyruvate availability for LDH, thus faster accumulation of lactate (i.e., glycolytic flux).

4.2. Enrichments of TCA Cycle Intermediates

To confirm that the inhibition of PDH was responsible for the observed effect, we employed stable isotope tracing to examine the enrichment of the TCA cycle intermediates. Stable isotope tracing is a powerful technique that enables the tracking of labeled atoms throughout metabolic pathways. However, before we present the enrichment data, we will provide a simplified overview of the routes through which pyruvate enters the TCA cycle, as well as the labeling patterns of pyruvate, lactate, and TCA cycle intermediates when using $[^{13}C_6]$glucose tracer (Fig. 9). When an [M + 6]glucose undergoes glycolysis, two fully labeled [M + 3]pyruvate molecules are generated. [M + 3]pyruvate can either be converted to [M + 3]lactate or enter the TCA cycle via one of three routes. The first route involves the decarboxylation of [M+3]pyruvate by PDH to [M + 2]acetyl-CoA, which is then condensed with oxaloacetate to form [M + 2]citrate (blue circles). Subsequently, [M + 2]citrate is metabolized through the TCA cycle, resulting in the sequential production of [M + 2]isocitrate, [M + 2]α-ketoglutarate, [M + 2]succinyl-CoA, [M + 2]succinate, [M + 2]fumarate, [M + 2]malate, and [M + 2]oxaloacetate. On the other hand, the other two routes entail the carboxylation of [M+3]pyruvate by PC or ME, producing [M+3]oxaloacetate or [M+3]malate, respectively (red circles), which are referred to as TCA cycle anaplerosis. The malate dehydrogenase and fumarase reactions interconvert oxaloacetate, malate, and fumarate, resulting in two labeling patterns due to the symmetry of fumarate. Finally, achieving higher-order labeling of the TCA cycle intermediates (e.g., [M + 5]α-ketoglutarate) involves multiple rounds of the TCA cycle and the contribution of anaplerosis.
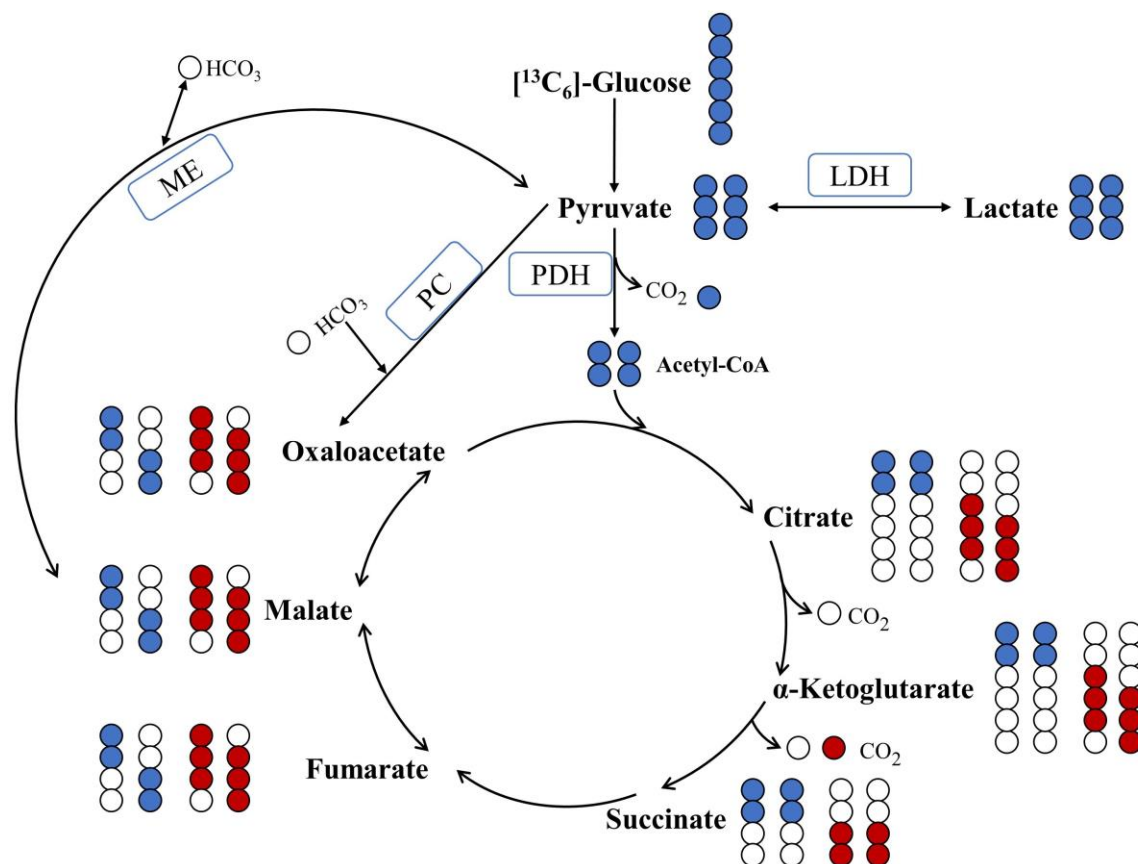
Fig. 9. A diagram illustrating the labeling pattern of pyruvate, lactate, and tricarboxylic acid (TCA) cycle intermediates when [$^{13}C_6$]glucose tracer is employed. Blue circles in pyruvate and lactate indicate ^{13}C atoms from [$^{13}C_6$]glucose that have undergone glycolysis, whereas blue circles in TCA cycle intermediates show carbon atoms introduced as labeled acetyl-CoA through pyruvate dehydrogenase (PDH). Red circles in TCA cycle intermediates signify carbon atoms that were derived through anaplerosis (i.e., pyruvate carboxylase [PC] and malic enzyme [ME]). White circles represent unlabeled carbon atoms.

In our second *in vitro* experiment, only two treatments were tested: control and CPI-613. This allowed us to specifically examine the effect of PDH inhibition, as PC inhibition showed no effect. All α-ketoglutarate isotopomers, [M + 1], [M + 2], [M + 3], [M + 4], and [M + 5], were detectable in the *in vitro* model of both treatments (Fig. 10). The labeling pattern of α-ketoglutarate showed a considerable appearance of the [M + 1] isotopomer (Fig. 10A), with a corresponding decrease in the appearance as the order of labeling

increased from [M + 1] to [M + 5]. A treatment, time, and treatment × time effects ($P <$

0.0001) were observed for [M + 2] (Fig. 10B), [M + 3] (Fig. 10C), [M + 4] (Fig. 10D), and

[M + 5]α-ketoglutarate (Fig. 10E), while only treatment and time effects ($P = 0.02$) were

detected for [M + 1]α-ketoglutarate. There were no differences between treatments in the

enrichment of [M+1]α-ketoglutarate at any time point. At 240 and 1440 min, lower [M + 2]

($P \leq 0.0003$) and [M+5]α-ketoglutarate ($P \leq 0.0004$) enrichments were observed for the

CPI-613 treatment compared to the control. Similarly, CPI-613-containing samples

exhibited reduced enrichments at 120, 240, and 1440 min for [M + 3] ($P \leq 0.02$) and

[M+4]α-ketoglutarate ($P \leq 0.04$) compared to controls.
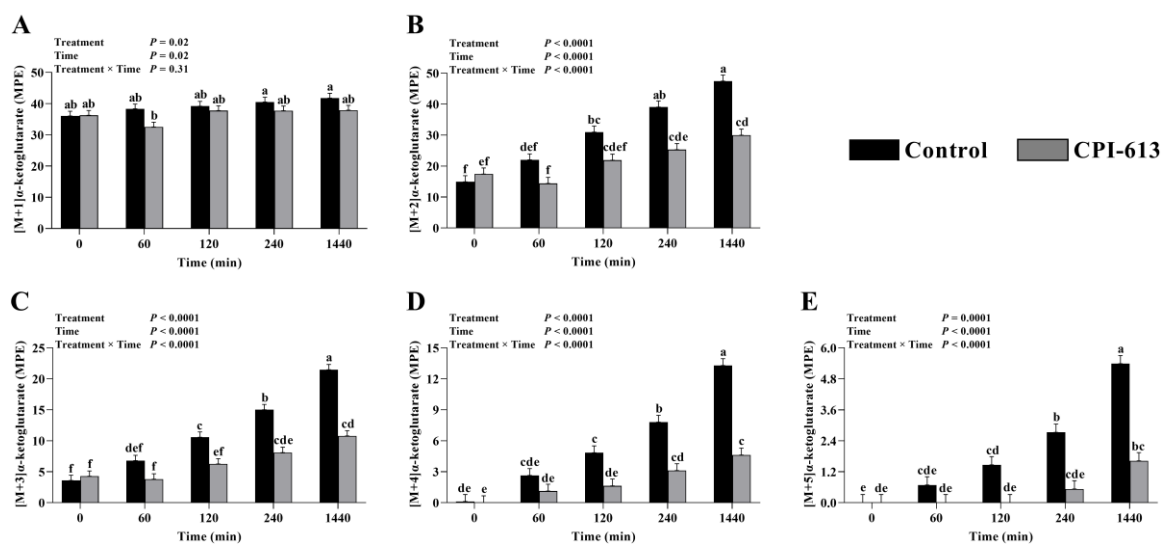
Fig. 10. α-ketoglutarate isotopomer enrichment of the *in vitro* model. [M+1]α-ketoglutarate enrichment (MPE; A), [M+2]α-ketoglutarate enrichment (MPE; B), [M+3]α-ketoglutarate enrichment (MPE; C), [M+4]α-ketoglutarate enrichment (MPE; D), and [M+5]α-ketoglutarate enrichment (MPE; E). Data are LS means ± SE. [a,b,c,d,e,f]Means lacking a common letter differ within a time point ($P \leq 0.05$).
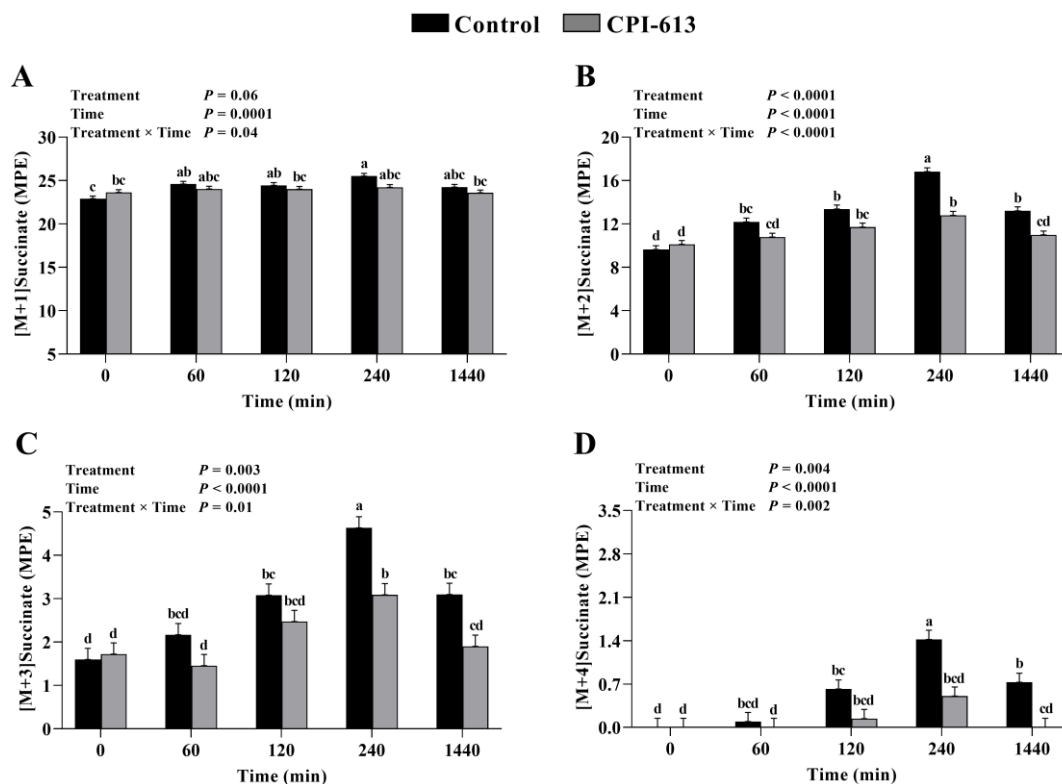
Fig. 11. Succinate isotopomer enrichment of the *in vitro* model. [M+1]succinate enrichment (MPE; A), [M+2]succinate enrichment (MPE; B), [M+3]succinate enrichment (MPE; C), and [M+4]succinate enrichment (MPE; D). Data are LS means ± SE. [a,b,c,d]Means lacking a common letter differ within a time point ($P \leq 0.05$).

Although a significant interaction effect was observed ($P = 0.04$) for [M+1]succinate (Fig. 11A), there were no differences among treatments in the enrichment of this isotopomer at any time point. Enrichment of [M + 2]succinate was significantly affected by treatment, time, and their interaction ($P < 0.0001$, Fig. 11B). A lower enrichment of [M + 2]α-ketoglutarate was detected at 240 ($P < 0.0001$) and 1440 min ($P = 0.002$) in reactions containing CPI-613 than the control. Significant treatment ($P = 0.003$), time ($P < 0.0001$), and treatment × time ($P = 0.01$) effects were also detected for [M+3]succinate (Fig. 11C). Yet, only at 240 min, a difference in the enrichment of [M+3]succinate ($P = 0.003$) was seen between treatments, in which the CPI-613 treatment had lower enrichment

than the control. Although [M+4]succinate enrichment generally remained <1 MPE, a treatment × time interaction was significant ($P = 0.002$, Fig. 11D). The inclusion of CPI-613 in the *in vitro* model lowered the enrichment of [M+4]succinate at 240 ($P = 0.002$) and 1440 min ($P = 0.03$) when compared to the control.

A time effect was observed for the *in vitro* model [M+1]fumarate enrichment ($P < 0.0001$, Fig 12A), in which an increase in the enrichment was observed over time. The enrichment of [M+2] (Fig. 12B), [M+3] (Fig. 12C), and [M+4]fumarate (Fig. 12B) were found to be significantly affected by treatment ($P \leq 0.02$), time ($P < 0.0001$), and their interaction ($P \leq 0.02$). There were no variations in the enrichments of [M+2], [M+3], and [M+4]fumarate at 0, 60, 120, and 240 min. Nonetheless, greater enrichments of all these isotopomers were seen at 1440 ($P \leq 0.02$) in the CPI-613 treatment compared to the control.

Fig. 12. Fumarate isotopomer enrichment of the *in vitro* model. [M+1]fumarate enrichment (MPE; A), [M+2]fumarate enrichment (MPE; B), [M+3]fumarate enrichment (MPE; C), and [M+4]fumarate enrichment (MPE; D). Data are LS means ± SE. [a,b,c,d,e,f]Means lacking a common letter differ within a time point ($P \leq 0.05$).

The enrichment of [M+1] (Fig. 13A), [M+2] (Fig. 13B), [M+3] (Fig. 13C), and [M+4]malate (Fig. 13D) were significantly affected by treatment ($P \leq 0.003$), time ($P < 0.0001$), and treatment × time ($P \leq 0.04$). At 240 and 1440 min, reaction vessels containing CPI-613 had lower [M+1]malate ($P \leq 0.006$) in comparison to controls. Greater enrichment of [M + 2]malate was detected at 240 and 1440 min in the CPI-613 treatment ($P \leq 0.02$) compared to the control. At 1440 min, the CPI-613 treatment had lower [M + 3] ($P = 0.02$) and [M+4]malate ($P = 0.002$) enrichments than the control.
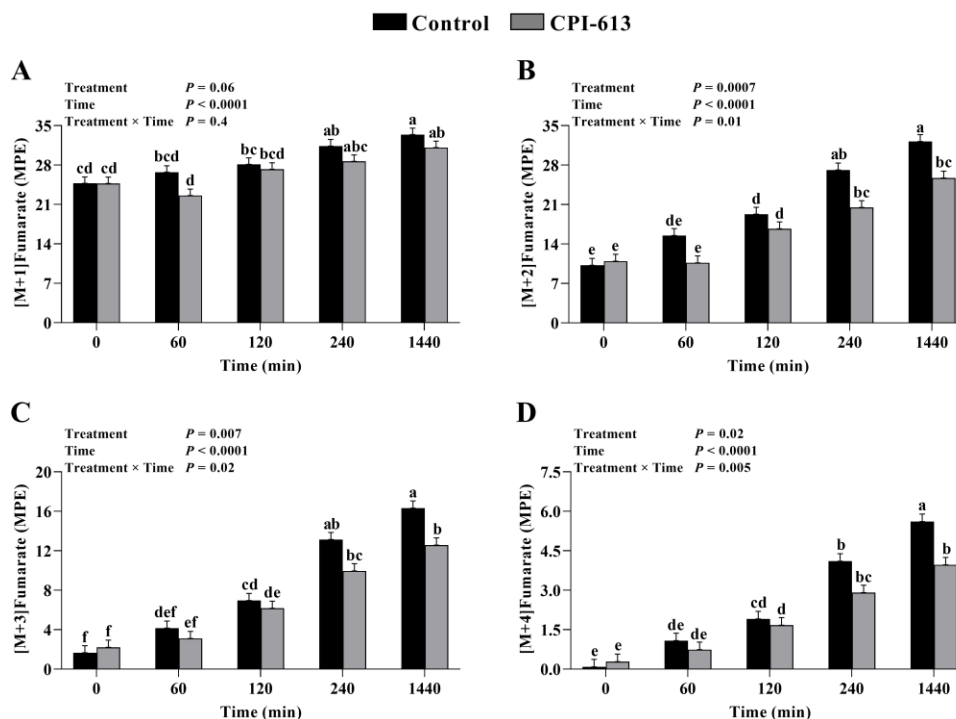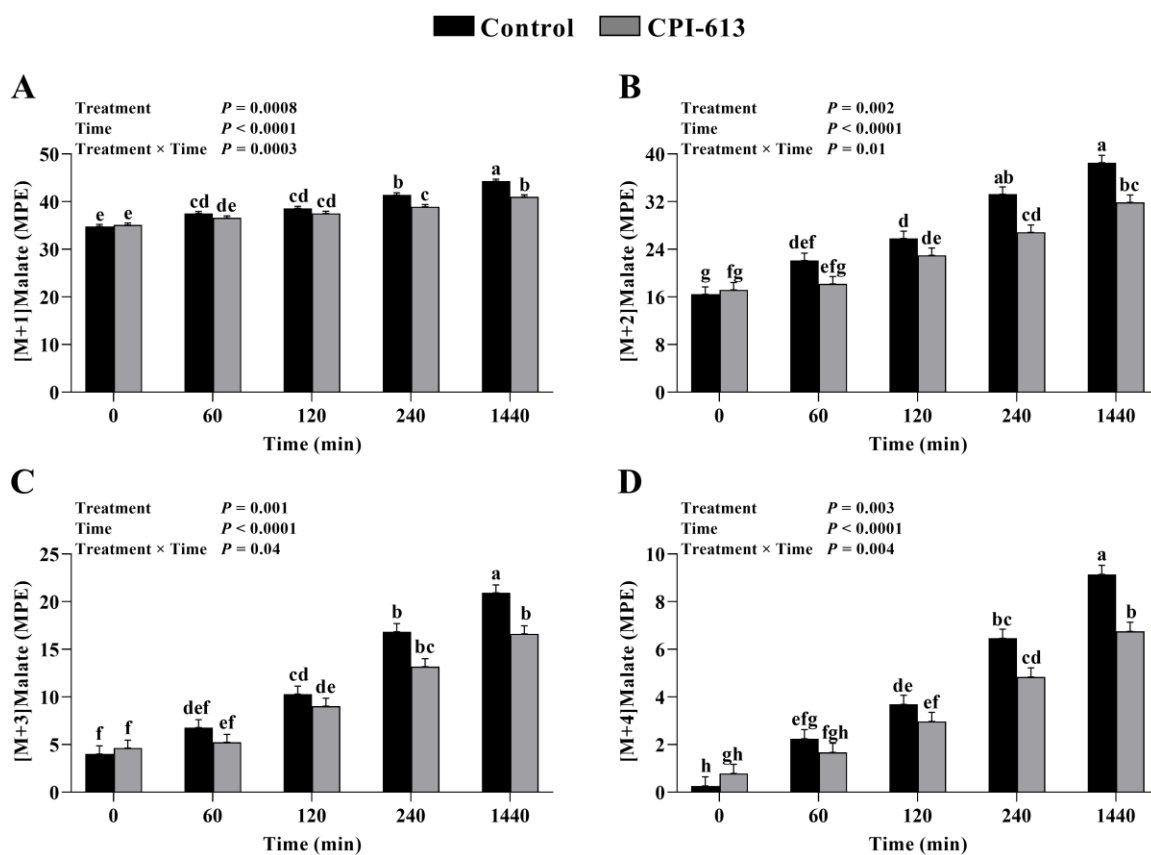

Fig. 13. Malate isotopomer enrichment of the *in vitro* model. [M+1]malate enrichment (MPE; A), [M+2]malate enrichment (MPE; B), [M+3]malate enrichment (MPE; C), and [M+4] malate enrichment (MPE; D). Data are LS means ± SE. [a,b,c,d,e,f,g]Means lacking a common letter differ within a time point ($P \leq 0.05$).

Owing to a number of factors, such as the presence of intermediates at low concentrations, lack of volatility, or degradation upon heat exposure during the chromatographic separation, it was not possible to measure the enrichments of all the TCA cycle intermediates. The current study compared the enrichment of all α-ketoglutarate, succinate, fumarate, and malate isotopomers between the CPI-613 and control treatments. The [M+1] isotopomers of all four intermediates had the highest abundance at 0 min and maintained relatively constant enrichment through the 1440 min period. The presence of enriched isotopomers at 0 min can be attributed to the naturally existing ^{13}C carbons in the muscle. This could also be due, in part, to enrichment that could have occurred during the homogenization of the muscle sample in the reaction buffer, which took place ~ 2 min before collecting the 0 min sample and subjecting it to PCA treatment. Unlike [M+1] isotopomers, the higher-order labeling isotopomers, [M+2] – [M+5], of all four intermediates showed an increase in enrichment over time. However, there was a decrease in the enrichment level with an increase in the labeling order. This was expected because achieving higher order-labeling patterns mandates multiple TCA cycle rounds and the involvement of anaplerosis. The second most abundant isotopomer of all intermediates was the [M+2]. All [M+2]isotopomers can be generated from [M+3]pyruvate via one round of the TCA cycle; [M+3]pyruvate is metabolized to [M+2]acetyl-CoA, which subsequently generates the [M+2] isotopomer of all the TCA cycle intermediate (from citrate to oxaloacetate). In the present study, [M+3]pyruvate was the most abundant isotopomer (data not shown), likely explains the high levels of [M + 2]α-ketoglutarate, succinate, fumarate, and malate.

The relative labeling of the TCA cycle intermediates can also provide insight into the

relative activities of PDH and PC. A greater proportion of [M+2] isotopomers compared to higher-order labeling isotopomers indicate that PDH was more active than PC. However, the progressive increase in the enrichment of [M+3], [M+4], and [M+5] isotopomers over time indicates that anaplerosis was maintained throughout the experiment. Interestingly, the activity of PDH was greater than PC in the CPI-613 treatment, despite the partial inhibition of PDH. A comparison of the enrichment of [M+2] isotopomers reveals that the enrichment of [M+2]succinate decreased to roughly half that of [M + 2]α-ketoglutarate in both treatments. This is likely a function of the entry of unlabeled metabolites (e.g., amino acids) at the succinyl-CoA level. Conversely, the subsequent increase in the enrichment of [M+2]fumarate and [M+2]malate compared to [M+2]succinate is likely through the function of PC and malic enzyme, as they were not inhibited in this experiment.

Our data indicate that the CPI-613 treatment lowered the enrichment of most α-ketoglutarate, succinate, fumarate, and malate isotopomers, mainly at 240 and 1440 min. It is important to point out that stable isotope tracing operates on the fact that any decline in metabolite enrichment results from dilution caused by unlabeled metabolites. As such, the decline in the enrichment of TCA cycle intermediates in the CPI-613-containing tubes is likely due to receiving an additional amount of unlabeled metabolites. This most likely occurred at the level of α-ketoglutarate, in which additional unlabeled α-ketoglutarate was produced from glutamate or glutamine. In totality, inhibition of PDH by CPI-613 appears to promote more incorporation of unlabeled intermediates to the TCA cycle, effectively decreasing the enrichment of many intermediates.

4.3. Enzymatic Activity

To rule out the possibility that the acceleration of pH decline in reactions containing

CPI-613 was not due to an increase in the activity of enzymes involved in glycogenolysis and glycolysis, we evaluated the activities of GP, PFK, and PK in the presence or absence of 400 µM CPI-613. GP is the rate-limiting enzyme of glycogenolysis that catalyzes the phosphorolytic degradation of glycogen. Glycogen phosphorylase has two forms: a and b, with b being the inactive form in skeletal muscle, whereas a is the active form (Newgard, Hwang, & Fletterick, 1989). PFK is the rate-limiting enzyme of glycolysis that converts fructose-6-phosphate and ATP to fructose-1,6-bisphosphate and ADP. Finally, PK is another regulatory enzyme of glycolysis that catalyzes the conversion of phosphoenolpyruvate and ADP to pyruvate and ATP.

The results indicate that there was no significant difference between treatments in the activity of the three tested enzymes (Table 1). The PFK, GPt, GPa, and PK activity levels were similar to those previously reported in porcine *longissimus* muscle(England, Matarneh, Scheffler, & Gerrard, 2014; Wang *et al*., 2020; Werner, Natter, & Wicke, 2010). These findings affirm that CPI-613 did not boost glycolytic flux by increasing the activity of key regulatory enzymes in glycogenolysis or glycolysis pathways. Rather, likely through providing more substrate for glycolysis.

Table 1. Enzymatic activities of Phosphoglucoisomerase (PFK), glycogen phosphorylase (GP) and pyruvate kinases (PK). All activities are expressed as µmol NADH $* \min^{-1} * $ g.

Enzymatic	Treatment	Values	*P*-Values
GPt	Control CPI-613	320.3 ± 27.1 295.0 ± 37.5	$P = 0.26$
GPa	Control CPI-613	103.9 ± 5.4 112.8 ± 5.4	$P = 0.20$
PFK	Control CPI-613	503.1 ± 27.1 466.7 ± 25.5	$P = 0.09$
PK	Control CPI-613	52.5 ± 1.1 55.5 ± 1.1	$P = 0.94$

5. CONCLUSION

In conclusion, this study provides evidence that the inhibition of PDH using CPI-613 in an *in vitro* system significantly impacts postmortem metabolism. The inhibition of PDH promotes glycogenolysis and glycolysis, resulting in increased rates and extents of pH decline, greater glycogen degradation, and accumulation of glucose, G6P, and lactate. Conversely, inhibiting PC with Avidin did not affect these processes. Tests utilizing a glucose tracer found that inhibition of PDH by CPI-613 reduced the enrichment of α-ketoglutarate, succinate, fumarate, and malate isotopomers. CPI-613 treatment generally resulted in lower enrichments of certain isotopomers compared to the control, particularly at 240 and 1440 minutes. Furthermore, the addition of CPI-613 did not affect the enzymatic activity of key enzymes in glycogenolysis and glycolysis, suggesting that the observed effects were primarily due to the inhibition of pyruvate consumption by PDH. These findings highlight the potential of PDH inhibition as a strategy to modulate postmortem metabolism, giving us potential for the development of novel approaches for meat quality improvement or preservation. However, additional investigations are necessary to thoroughly comprehend the function of mitochondria in postmortem metabolism and its effect on the quality of meat.

REFERENCES

Adina-Zada, A., Zeczycki, T. N., & Attwood, P. V. (2012). Regulation of the structure and activity of pyruvate carboxylase by acetyl CoA. *Archives of Biochemistry and Biophysics*, *519*(2), pp.118–130.

Al-Qusairi, L., & Laporte, J. (2011). T-tubule biogenesis and triad formation in skeletal muscle and implication in human diseases. *Skeletal Muscle*, *1*(1), pp. 1–11.

Alistar, A., Morris, B. B., Desnoyer, R., Klepin, H. D., Hosseinzadeh, K., Clark, C., Cameron, A., Leyendecker, J., D'Agostino, R., Topaloglu, U., Boteju, L. W., Boteju, A. R., Shorr, R., Zachar, Z., Bingham, P. M., Ahmed, T., Crane, S., Shah, R., Migliano, J. J., … Pasche, B. (2017). Safety and tolerability of the first-in-class agent CPI-613 in combination with modified FOLFIRINOX in patients with metastatic pancreatic cancer: a single-centre, open-label, dose-escalation, phase 1 trial. *The Lancet Oncology*, *18*(6), pp. 770–778.

Attwood, P. V., Mayer, F., & Wallace, J. C. (1986). Avidin as a probe of the conformational changes induced in pyruvate carboxylase by acetyl-CoA and pyruvate. *FEBS Letters*, *203*(2), pp. 191–196.

Beltrán, J. A., Jaime, I., Santolaria, P., Sañudo, C., Albertí, P., & Roncalés, P. (1997). Effect of stress-induced high post-mortem pH on protease activity and tenderness of beef. *Meat Science*, *45*(2), pp. 201–207.

Bendall, J. R. (1979). Relations between muscle pH and important biochemical parameters during the postmortem changes in mammalian muscles. *Meat Science*, *3*(2), pp. 143–157.

Bergmeyer, H. U. (1984). *(3rd ed.). Methods of enzymatic analysis, vol. 6. Weinheim: Verlag Chemie.*

Bouton, P. E., Harris, P. V., & Shorthose, W. R. (1971). Effect of ultimate pH upon the water-holding capacity and tenderness of mutton. *Journal of Food Science*, *36*(3), pp. 435–439.

Bremer, J., & Davis, E. J. (1975). Studies on the active transfer of reducing equivalents into mitochondria via the malate-aspartate shuttle. *BBA - Bioenergetics*, *376*(3), pp. 387–397.

Bricker, D. K., Taylor, E. B., Schell, J. C., Orsak, T., Boutron, A., Chen, Y. C., Cox, J. E., Cardon, C. M., Van Vranken, J. G., Dephoure, N., Redin, C., Boudina, S., Gygi, S. P., Brivet, M., Thummel, C. S., & Rutter, J. (2012). A mitochondrial pyruvate carrier required for pyruvate uptake in yeast, Drosophila, and humans. *Science*, *336*(6090), pp. 96–100.

Calder, P. C., & Geddes, R. (1990). Post mortem glycogenolysis is a combination of phosphorolysis and hydrolysis. *International Journal of Biochemistry*, *22*(8), pp. 847–856.

den Hertog-Meischke, M. J. A., van Laack, R. J. L. M., & Smulders, F. J. M. (1997). The water-holding capacity of fresh meat. *Veterinary Quarterly*, *19*(4), 175–181.

Des Rosiers, C., Di Donato, L., Comte, B., Laplante, A., Marcoux, C., David, F., Fernandez, C. A., & Brunengraber, H. (1995). Isotopomer analysis of citric acid cycle and gluconeogenesis in rat liver. Reversibility of isocitrate dehydrogenase and involvement of ATP-citrate lyase in gluconeogenesis. *The Journal of Biological*

Chemistry, *270*(17), pp. 10027–10036.

Dettmer, K., Aronov, P. A., & Hammock, B. D. (2007). Mass spectrometry-based metabolomics. *Mass Spectrometry Reviews*, *26*(1), pp. 51–78.

Dong, M., Chen, H., Zhang, Y., Xu, Y., Han, M., Xu, X., & Zhou, G. (1947). Processing Properties and Improvement of Pale, Soft, and Exudative-Like Chicken Meat: a Review.

Dörsam, B., & Fahrer, J. (2016). The disulfide compound α-lipoic acid and its derivatives: A novel class of anticancer agents targeting mitochondria. *Cancer Letters*, *371*(1), pp. 12–19.

El-Aneed, A., Cohen, A., & Banoub, J. (2009). Mass Spectrometry, Review of the Basics: Electrospray, MALDI, and Commonly Used Mass Analyzers. *Applied Spectroscopy Reviews*, *44*(3), pp. 210–230.

El-Kadi, S. W., Baldwin, R. L., McLeod, K. R., Sunny, N. E., & Bequette, B. J. (2009). Glutamate Is the Major Anaplerotic Substrate in the Tricarboxylic Acid Cycle of Isolated Rumen Epithelial and Duodenal Mucosal Cells from Beef Cattle. *The Journal of Nutrition*, *139*(5), pp. 869–875.

Endo, M. (1977). Calcium release from the sarcoplasmic reticulum. *Physrev.* *57*(1), pp. 71–108.

England, E. M., Matarneh, S. K., Mitacek, R. M., Abraham, A., Ramanathan, R., Wicks, J. C., Shi, H., Scheffler, T. L., Oliver, E. M., Helm, E. T., & Gerrard, D. E. (2018). Presence of oxygen and mitochondria in skeletal muscle early postmortem. *Meat Science*, *139*, pp. 97–106.

England, E. M., Matarneh, S. K., Scheffler, T. L., & Gerrard, D. E. (2017). Perimortal Muscle Metabolism and its Effects on Meat Quality. *New Aspects of Meat Quality*, pp. 63–89.

England, E. M., Matarneh, S. K., Scheffler, T. L., Wachet, C., & Gerrard, D. E. (2014). pH inactivation of phosphofructokinase arrests postmortem glycolysis. *Meat Science*, *98*(4), pp. 850–857.

Feliu, J. E., Hue, L., & Hers, H. G. (1976). Hormonal control of pyruvate kinase activity and of gluconeogenesis in isolated hepatocytes. *Proceedings of the National Academy of Sciences of the United States of America*, *73*(8), pp. 2762–2766.

Fernandez, C. A., Rosiers, C. Des, Previs, S. F., David, F., & Brunengraber, H. (1996). Correction of13C Mass Isotopomer Distributions for Natural Stable Isotope Abundance. *Journal of Mass Spectrometry*, *31*(3), pp. 255–262.

Fujii, J., Otsu, K., Zorzato, F., De Leon, S., Khanna, V. K., Weiler, J. E., O'Brien, P. J., & Maclennan, D. H. (1991). Identification of a Mutation in Porcine Ryanodine Receptor Associated with Malignant Hyperthermia. *Science*, *253*(5018), pp. 448–451.

Gao, X., Xie, L., Wang, Z., Li, X., Luo, H., Ma, C., & Dai, R. (2013). Effect of postmortem time on the metmyoglobin reductase activity, oxygen consumption, and colour stability of different lamb muscles. *European Food Research and Technology*, *236*(4), pp. 579–587.

Gray, L. R., Tompkins, S. C., & Taylor, E. B. (2014). Regulation of pyruvate metabolism and human disease. *Cellular and Molecular Life Sciences*, *71*(14), pp. 2577–2604.

Hamm, R. (1986). Functional properties of the myofibrillar system and their measurements.

Hammelman, J. E., Bowker, B. C., Grant, A. L., Forrest, J. C., Schinckel, A. P., & Gerrard, D. E. (2003). Early postmortem electrical stimulation simulates PSE pork development. *Meat Science*, *63*(1), pp. 69–77.

Haslam, J. M., & Krebs, H. A. (1968). The permeability of mitochondria to oxaloacetate and malate. *Biochemical Journal*, *107*(5), pp. 659–667.

Heart, E., Cline, G. W., Collis, L. P., Pongratz, R. L., Gray, J. P., & Smith, P. J. S. (2009). Role for malic enzyme, pyruvate carboxylation, and mitochondrial malate import in glucose-stimulated insulin secretion. *American Journal of Physiology - Endocrinology and Metabolism*, *296*(6), pp. 1354–1362.

Hoppeler, H., Vogt, M., Weibel, E. R., & Flück, M. (2003). Response of skeletal muscle mitochondria to hypoxia. *Experimental Physiology*, *88*(1), pp. 109–119.

Hughes, J. M., Oiseth, S. K., Purslow, P. P., & Warner, R. D. (2014). A structural approach to understanding the interactions between colour, water-holding capacity and tenderness. *Meat Science*, *98*(3), pp. 520–532.

Jafary, F., Ganjalikhany, M. R., Moradi, A., Hemati, M., & Jafari, S. (2019). Novel Peptide Inhibitors for Lactate Dehydrogenase A (LDHA): A Survey to Inhibit LDHA Activity via Disruption of Protein-Protein Interaction. *Scientific Reports 2019 9:1*, *9*(1), pp. 1–13.

JOHANNSSEN, W., ATTWOOD, P. V., WALLACE, J. C., & KEECH, D. B. (1983). Localisation of the Active Site of Pyruvate Carboxylase by Electron Microscopic Examination of Avidin-Enzyme Complexes. *European Journal of Biochemistry*, *133*(1), pp. 201–206.

Klont, R. E., Brocks, L., & Eikelenboom, G. (1998). Muscle fibre type and meat quality. *Meat Science*, *49*(SUPPL. 1), pp. S219–S229.

Kowalski, G. M., De Souza, D. P., Burch, M. L., Hamley, S., Kloehn, J., Selathurai, A., Tull, D., O'Callaghan, S., McConville, M. J., & Bruce, C. R. (2015). Application of dynamic metabolomics to examine in vivo skeletal muscle glucose metabolism in the chronically high-fat fed mouse. *Biochemical and Biophysical Research Communications*, *462*(1), pp. 27–32.

Küchenmeister, U., Kuhn, G., Wegner, J., Nürnberg, G., & Ender, K. (1999). Post mortem changes in Ca2+ transporting proteins of sarcoplasmic reticulum in dependence on malignant hyperthermia status in pigs. *Molecular and Cellular Biochemistry 1999 195:1*, *195*(1), pp. 37–46.

Luther, P. K. (2009). The vertebrate muscle Z-disc: Sarcomere anchor for structure and signalling. *Journal of Muscle Research and Cell Motility*, *30*(5–6), pp. 171–185.

Marcinek, D. J., Kushmerick, M. J., & Conley, K. E. (2010). Lactic acidosis in vivo: testing the link between lactate generation and H^+ accumulation in ischemic mouse muscle. *Journal of Applied Physiology*, *108*(6), pp. 1479–1486.

Matarneh, S. K., Beline, M., de Luz e Silva, S., Shi, H., & Gerrard, D. E. (2018). Mitochondrial F1-ATPase extends glycolysis and pH decline in an in vitro model. *Meat Science*, *137*, pp. 85–91.

Matarneh, S. K., England, E. M., Scheffler, T. L., & Gerrard, D. E. (2017). The Conversion of Muscle to Meat. *Lawrie's Meat Science: Eighth Edition*, pp. 159–185.

Matarneh, S. K., England, E. M., Scheffler, T. L., Yen, C. N., Wicks, J. C., Shi, H., & Gerrard, D. E. (2017). A mitochondrial protein increases glycolytic flux. *Meat Science*, *133*, pp. 119–125.

Matarneh, S. K., Silva, S. L., & Gerrard, D. E. (2021). New Insights in Muscle Biology that Alter Meat Quality. *9*, pp. 355–377.

Matarneh, S. K., Yen, C. N., Bodmer, J., El-Kadi, S. W., & Gerrard, D. E. (2021). Mitochondria influence glycolytic and tricarboxylic acid cycle metabolism under postmortem simulating conditions. *Meat Science*, *172*, 108316.

McCommis, K. S., & Finck, B. N. (2015). Mitochondrial pyruvate transport: a historical perspective and future research directions. *Biochemical Journal*, *466*(3),pp 443–454.

Mickelson, J. R., & Louis, C. F. (1996). Malignant hyperthermia: excitation-contraction coupling, Ca2+ release channel, and cell Ca2+ regulation defects, *76*(2), pp. 537–592.

Miller, M. F., Carr, M. A., Ramsey, C. B., Crockett, K. L., & Hoover, L. C. (2001). Consumer thresholds for establishing the value of beef tenderness. *Journal of Animal Science*, *79*(12), pp. 3062–3068.

Molette, C., Rémignon, H., & Babilé, R. (2003). Maintaining muscles at a high post-mortem temperature induces PSE-like meat in turkey. *Meat Science*, *63*(4), pp. 525–532.

Newgard, C. B., Hwang, P. K., & Fletterick, R. J. (1989). The family of glycogen phosphorylases: Structure and functio. *Critical Reviews in Biochemistry and Molecular Biology*, *24*(1), pp. 69–99.

Newton, K. G., & Gill, C. O. (1981). The microbiology of DFD fresh meats: A review. *Meat Science*, *5*(3), pp. 223–232.

Patel, M. S., & Korotchkina, L. G. (2006). Regulation of the pyruvate dehydrogenase complex. *Biochemical Society Transactions*, *34*(2), pp. 217–222.

Petracci, M., Bianchi, M., & Cavani, C. (2009). The European perspective on pale, soft, exudative conditions in poultry. *Poultry Science*, *88*(7), pp. 1518–1523.

Purslow, P. P. (2020). The Structure and Role of Intramuscular Connective Tissue in Muscle Function. *Frontiers in Physiology*, *11*, 495.

Robergs, R. A., Ghiasvand, F., & Parker, D. (2004). Biochemistry of exercise-induced metabolic acidosis. *American Journal of Physiology - Regulatory Integrative and Comparative Physiology*, *287*(3 56-3).

Scheffler, T. L., & Gerrard, D. E. (2007). Mechanisms controlling pork quality development: The biochemistry controlling postmortem energy metabolism. *Meat Science*, *77*(1), pp. 7–16.

Scheffler, T. L., Park, S., & Gerrard, D. E. (2011). Lessons to learn about postmortem metabolism using the AMPKγ3R200Q mutation in the pig. *Meat Science*, *89*(3), pp. 244–250.

Schneider, M. F. (1994). Ccontrol of calcium release in functioning skeletal muscle fibers. *Annu. Rev. Physiol*, *56*, pp. 463–484.

Schwägele, F., Haschke, C., Honikel, K. O., & Krauss, G. (1996). Enzymological investigations on the causes for the PSE-syndrome, I. Comparative studies on pyruvate kinase from PSE- and normal pig muscles. *Meat Science*, *44*(1–2), pp. 27–40.

Scopes, R. K. (1974). Studies with a reconstituted muscle glycolytic system. The rate and extent of glycolysis in simulated post-mortem conditions. *Biochemical Journal*, *142*(1), pp. 79–86.

Sheeran, F. L., Angerosa, J., Liaw, N. Y., Cheung, M. M., & Pepe, S. (2019). Adaptations in protein expression and regulated activity of pyruvate dehydrogenase multienzyme

complex in human systolic heart failure. *Oxidative Medicine and Cellular Longevity*, *2019*.

Skorkowski, E. F. (1988). Mitochondrial malic enzyme from crustacean and fish muscle. *Comparative Biochemistry and Physiology. B, Comparative Biochemistry*, *90*(1), pp. 19–24.

Solomon, M. B., Van Laack, R. L. J. M., & Eastridge, J. S. (1998). Biophysical basis of pale, soft, exudative (PSE) pork and poultry muscle: a review. *Journal of Muscle Foods*, *9*(1), pp. 1–11.

Swatland, H. J. (2008). How pH causes paleness or darkness in chicken breast meat. *Meat Science*, *80*(2), pp. 396–400.

Trivedi, B. (1966). Effect of pH on the kinetics of frog muscle phosphofructokinase. *Journal of Biological Chemistry*, *241*, pp. 4110–4114.

Valvona, C. J., Fillmore, H. L., Nunn, P. B., & Pilkington, G. J. (2016). The Regulation and Function of Lactate Dehydrogenase A: Therapeutic Potential in Brain Tumor. *Brain Pathology*, *26*(1), pp. 3–17.

Van Wezemael, L., De Smet, S., Ueland, Ø., & Verbeke, W. (2014). Relationships between sensory evaluations of beef tenderness, shear force measurements and consumer characteristics. *Meat Science*, *97*(3), pp. 310–315.

Wang, Y., Liu, R., Hou, Q., Tian, X., Fan, X., Zhang, W., & Zhou, G. (2020). Comparison of activity, expression and S-nitrosylation of glycolytic enzymes between pale, soft and exudative and red, firm and non-exudative pork during post-mortem aging. *Food Chemistry*, *314*, 126203.

Werner, C., Natter, R., & Wicke, M. (2010). Changes of the activities of glycolytic and oxidative enzymes before and after slaughter in the longissimus muscle of Pietrain and Duroc pigs and a Duroc-Pietrain crossbreed1. *Journal of Animal Science*, *88*(12), pp. 4016–4025.

CURRICULUM VITAE

Mackenzie Taylor M.S.

Department of Nutrition, Dietetics and Food Sciences
Utah State University
Logan, UT 84322-8700
Phone (801) 888-7095
kenzie.taylor@usu.edu

Education

2021 – Present	M.S.	Utah State University, UT Food Science (emphasis: Meat Science/Muscle Biology)
2017 – 2021	B.S.	Utah State University, UT Animal, Dairy, and Veterinary Science

Research Experience

2021 – Present	**Graduate Research Assistant** Utah State University, Department of Nutrition, Dietetics, and Food Sciences
2020 – 2021	**Research Assistant** Utah State University, Department of Nutrition, Dietetics, and Food Sciences

Scholarships and Awards

2023	IFT College Bowl Team Competition 2nd place winner
2023	Ocean Spray Product Research and Development Competition top 4
2022	Ocean Spray Product Research and Development Competition 1st place ($5,000)
2022	National Dairy Council Product Research and Development Competition 1st place ($8,000)
2022	IFT College Quiz Bowl Team Competition 4th place winner
2017 & 2020	Utah State University Dean's List

Research Support

2022 – 2024 **Studying the histological, ultrastructural, and physiochemical changes of frozen/thawed beef ribs**
PI – Sulaiman K. Matarneh

- I generated preliminary data and contributed to experimental design.

National Cattleman's Association
$70,701 awarded

2022 – 2023 **Dr. Niranjan R. Gandhi and Mrs. Josephine N Gandhi Food Science Research Assistantship**
$20,00 awarded

Publications

Published/In Press/Submitted Articles

1. C. Wang, **M.J. Taylor**, C.D. Stafford**,** D.S. Dang, S.K. Matarneh, D.E. Gerrard. (2022). Analysis of phosphofructokinase activity as affected by pH and ATP concentration. *Currently submitted and under review in Journal of Biological Chemistry.* **Journal Impact Factor: 3.241**.

2. C.C Reichhardt*, C. D. Stafford**,** J. M., Cuthbert, Dang, D. S., Motsinger, L. A., **Taylor, M. J.**, Briggs, R. K., Brady, T. J., Thomas, A. J., Garcia, M. D., Matarneh, S. K., & Thornton, K. J. 2022. Cattle breed type and anabolic implants impact calpastatin expression and abundance of mRNA associated with protein turnover in the *longissimus thoracis* of feedlot steers. *Animal Science*, *100(8),* 1-11. doi.org/10.1093/JAS/SKAC204. **Journal Impact Factor: 3.338**.

3. C.D. Stafford**, M.J. Taylor***, D.S. Dang, E.M. England, D.P. Cornforth, X. Dai, S.K. Matarneh (2022). Spectro 1-A potential spectrophotometer for measuring color and myoglobin forms in beef. *Foods*. 11(14):2091. doi.org/10.3390/foods11142091. **Journal Impact Factor: 5.561**.

4. D.S. Dang, C.D. Stafford, **M.J. Taylor**, J.F. Buhler, K.J. Thornton, S.K. Matarneh. (2022). Ultrasonication of beef improves calpain-1 autolysis and caspase-3 activity by elevating cytosolic calcium and inducing mitochondrial dysfunction. *Meat Science, 183*:108646. **Journal Impact Factor: 7.077**.

Presentations at Professional Meetings

Underlined font indicates presenting author. Presentations are listed in chronological (by year and month) order.

National Meetings
1. <u>C.D. Stafford</u>, **M.J. Taylor**, D.S. Dang, K.J. Thornton, S.K. Matarneh. Freezing Improves Meat Tenderness by Enhancing Postmortem Proteolysis. 75th *Reciprocal Meat Conference.* June 2022, Des Moines, Iowa, USA.

2. **M.J. Taylor**, C.D. Stafford, D.S. Dang, S.K. Matarneh. Color Muse Spectro 1 as a Potential Spectrophotometer for Evaluating Color in Meat. 75th *Reciprocal Meat Conference.* June 2022, Des Moines, Iowa, USA.

3. <u>C.D. Stafford</u>, J.F. Buhler, D. S. Dang, **M.J. Taylor**, K.J. Thornton, S. K Matarneh Mitochondria calcium buffering limit postmortem proteolysis in an *in vitro* model. *74th Reciprocal Meat Conference.* August 2021, Reno, Nevada, USA.

4. <u>D.S. Dang</u>**,** C.D. Stafford, J.F. Buhler, **M.J. Taylor**, J.E. Shippen, S.K. Matarneh. Ultrasonication of meat enhances the activity of several proteolytic systems involved in postmortem proteolysis and tenderization. 74th *Reciprocal Meat Conference.* August 2021, Reno, Nevada, USA.

5. **M.J. Taylor**, J.F. Buhler, C.D. Stafford, D.S. Dang, S.W. El-Kadi, D.E. Gerrard, S.K. Matarneh. Inhibition of pyruvate dehydrogenase accelerates anaerobic glycolysis in an in vitro model. 74th *Reciprocal Meat Conference,* August 2021, Reno, NV, USA.

Regional Meetings
1. <u>A.K. Roberts</u>, <u>M. Garcia</u>, C.D. Stafford, **M.J. Taylor**, K.J. Thornton, S.K. Matarneh. Disrupted Mitochondria Influences Postmortem Proteolysis. *Research on Capital Hill*. January 2023. Salt Lake City, Utah.

2. **M.J. Taylor**, D.S. Dang, J.F. Buhler, C.D. Stafford, S.K. Matarneh. Mitochondria delay proteolysis in an *in vitro* model simulating postmortem conditions. *Utah State University Student Research Symposium*, Logan, Utah, USA. April 2021. Virtual.

Undergraduate students mentored

11/2022 - Present	Jessica Godinez, Animal, Dairy and Veterinary Sciences, USU
10/2021 - Present	Adam Roberts, Animal, Dairy and Veterinary Sciences, USU
10/2021 - Present	Micaela Garcia, Nutrition, Dietetics and Food Sciences, USU
10/2020 - 08/2021	Jordan Prestwich, Nutrition, Dietetics and Food Sciences, USU
10/2020 - 02/2021	Amber Thornton, Animal, Dairy and Veterinary Sciences, USU
10/2020 – 02/2021	Isabel Trent, Animal, Dairy and Veterinary Sciences, USU

Leadership

2022 - Present   USU Food Science Club Vice President

Professional Societies

American Meat Science Association (AMSA)

Bonneville Section Institute of Food Technologists (IFT)

Teaching Experience -TA

Utah State University

ADVS 2200- Anatomy and Physiology of Animals
(Fall 2018)

NDFS 5020/6020- Meat Technology and Processing
(Fall 2022)